THE MINISTRY OF NATIONAL INFRASTRUCTURES

GEOLOGICAL SURVEY OF ISRAEL

Description and Benchmarking of the 1D Multi-Component Chemistry-Based Model for the Dead Sea (1D-DS-POM)

Yona Dvorkin, Nadav G. Lensky,

Vladimir Lyakhovsky and Ittai Gavrieli

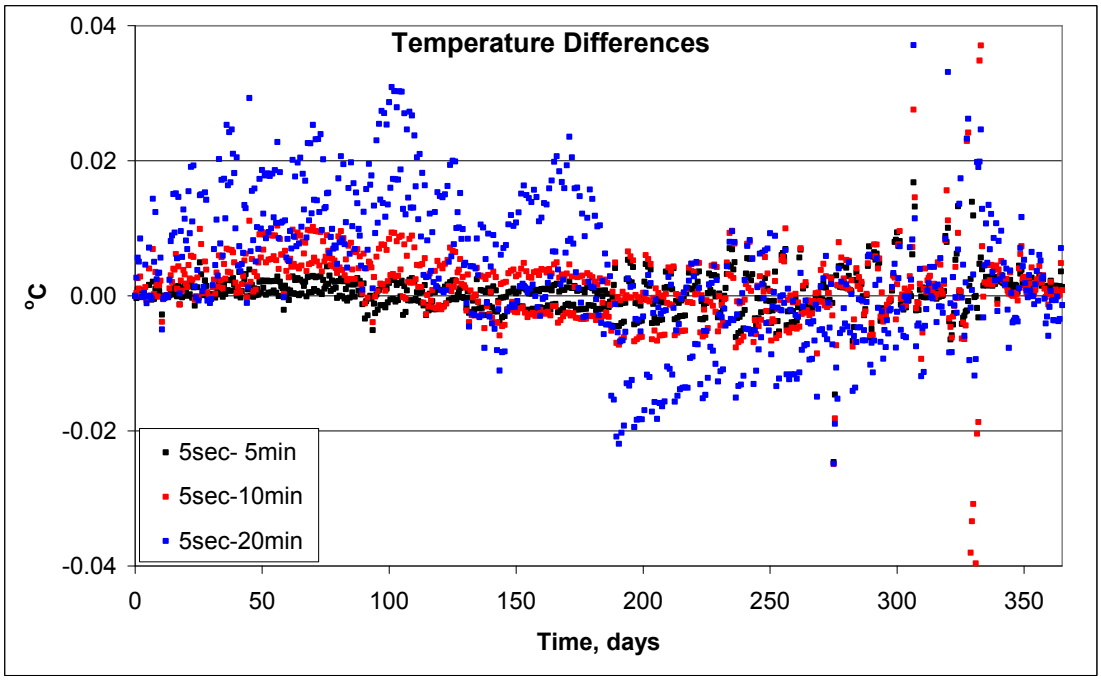

Jerusalem, December 2007 **GSI/15/2007**

THE MINISTRY OF NATIONAL INFRASTRUCTURES

GEOLOGICAL SURVEY OF ISRAEL

Description and Benchmarking of the 1D Multi-Component Chemistry-Based Model for the Dead Sea (1D-DS-POM)

Yona Dvorkin, Nadav G. Lensky,

Vladimir Lyakhovsky and Ittai Gavrieli

Jerusalem, December 2007 **GSI/15/2007**

Table of Contents

1 Introduction 3
2 Physical Processes and Balances 7
2.1 Heat Exchange 7
2.2 Heat and Mass Transport 8
2.3 Mass conservation 9
2.4 Inflows and Pumping 10
3 Thermodynamics and Chemical Processes 11
3.1 Units Conversions 12
3.1.1 Molality to Salinity 12
3.1.2 Salinity to Molality 12
3.2 Equation of State 13
3.3 Degree of Saturation 15
3.4 Salt Precipitation 15
4 Numerical Method 16
4.1 Grid Geometry 17
4.1.1 Grid Remeshing 22
4.2 Heat and Mass Transport 23
4.3 Time Step Selection 24
4.3.1 One year runs 24
4.3.2 52 year runs 28
5 Benchmarking 29
5.1 Heat Balance and Related Level Change 29
5.2 Mass balance 35
5.2.1 Salt Precipitation 35
5.2.2 Evaporation 38
5.2.3 Inflows 39
5.3 Compressible vs. Incompressible Models 43
6 Summary 45
7 References 46

Abstract

1D-DS-POM is a one dimensional, compressible, multi-component, chemistry-based limnological model for the Dead Sea. The model is a modification of the 1D Princeton Ocean Model (1D-POM) for the specific conditions of the Dead Sea. The model describes various physical and chemical processes which control the temperature distribution and the composition of the Dead Sea brine. The physical processes include heat exchange at the sea surface, turbulent and molecular vertical heat and mass transport, and various inflows that affect the Dead Sea now or may affect it in the future. Complex chemical composition and salt precipitation from the Dead Sea brine required the major modification of the 1D-POM, namely introduction of the eight principal chemical constituents instead of a single salinity. The model calculates brine density with a new equation of state, the degree of saturation for the considered salts (halite, gypsum and carnallite) and water activity using the Pitzer thermodynamic approach. The equation of state is capable of determining the density in the range from freshwater to the reject brines of the Dead Sea industries. Input to the model includes measured meteorological data, pumping by the chemical industries and predefined volumes of different inflow sources, including seawater. Here we present results of benchmarking simulations carried out for the main processes, which demonstrate the ability of the 1D-DS-POM to reproduce the Dead Sea structure and its dynamics under different scenarios.

1 Introduction

The rapid decline in the Dead Sea (DS) level over the past decades (25 meters since the 1960s and ~1 m/yr in the last decade), has become an environmental, social and economic concern in Israel and Jordan and has drawn the attention of the international community. One of the alternatives considered to raise and/or stabilize lake level is the construction of a Red Sea - Dead Sea conduit (RSDSC) that will pipe seawater from the Red Sea to the DS. The proposed project also includes a desalinization plant whereby the 400 meter elevation difference between the Seas will be utilized to desalinize seawater close the DS shores. The potable water will be pumped to Israel, Jordan and the Palestinian Authority, whereas the reject brine from desalinization will be discharged to the DS. Terms of reference (TOR) for a feasibility study for this project were signed by Israel, Jordan and the Palestinian Authority in 2005 and the study is expected to commence in 2007 under the management of the World Bank.

Mixing of seawater and DS brine will have major limnological geochemical and biological impacts on the lake (Gavrieli et al., 2002, Gavrieli et al., 2005). In order to evaluate and quantify these processes, on the **long-term** (decades), it is necessary to develop a dynamic limnological model for the DS that comprises the unique parameters which determine the behavior of the lake. However, standard oceanographic/limnological models are not suitable to simulate these processes because of the exceptional aspects that need to be considered. Among these are:

- Chemistry: The changing composition of the brine requires that the model follow the composition of the brine and not its salinity alone, as done in standard codes.
- Thermodynamics and salt precipitation: The model must include thermodynamic modules that determine the degree of saturation with respect to dissolved salts. When found to be oversaturated, the model needs to "precipitate" halite (NaCl, as occurs today) and gypsum ($CaSO_4$, as will occur if seawater will mix with the DS brine) until saturation is regained.
- An equation of state based on composition. The DS system spans over a huge range of densities and compositions, from freshwater and seawater through the DS brine to the much denser End Brines, which are the reject brine from the chemical industries that pump and evaporate DS brine. This range of densities requires the establishment of an equation of state that relates the density to the composition of the brine and not its salinity, in addition to the temperature.
- Evaporation as a function of salinity. To properly calculate the water and mass balances of the lake, the rate of evaporation, which is part of the heat balance of the lake, needs to be well constrained. This rate is a function of the salinity of the surface water, which changes continuously.
- The compressibility of the system under discussion needs to be evaluated when dealing with the above-mentioned large range of densities and compositions.

In light of the discussion of the RSDSC, the Geological Survey of Israel has undertaken to formulate a dynamic limnological model that would include the special features of the DS. First, the basic gaps in knowledge were identified (Gavrieli et al., 2002) followed by the establishment of the energy and mass balances of the lake (Lensky et al, 2005). Concurrently, biological and mixing experiments were initiated to attain better insight into the mechanism of biological blooming and the kinetics of

gypsum nucleation and crystal growth, respectively (Oren et al., 2004, 2005; Ganor et al., 2006). The latter is important as it will determine at what rate the gypsum crystals will settle to the seafloor thereby dictating the color of the surface waters.

Recently, a 1-dimentional model for the Dead Sea (1D-DS-POM) was completed and preliminary un-calibrated results were presented (Gavrieli et al., 2006). This multi-component chemistry-based model is based on the 1D-Princeton Oceanographic Model (POM), which was modified to include the processes described above, excluding the biology. In the current report we present an in-depth description of the underlying modules and chemical and physical processes included in the code. Fig 1.1 is a flow chart of 1D-DS-POM which allows the reader to follow the sequence of operation and the interaction between the various modules of the code. The final part of the report presents several benchmarking tests, which verify the accuracy of the numerical model. In the coming months the model will be calibrated and scenarios of seawater, reject brine and increased freshwater inflows would be evaluated. This will be followed by the formulation of a 2D model for the DS and the mixing of seawater in the lake.

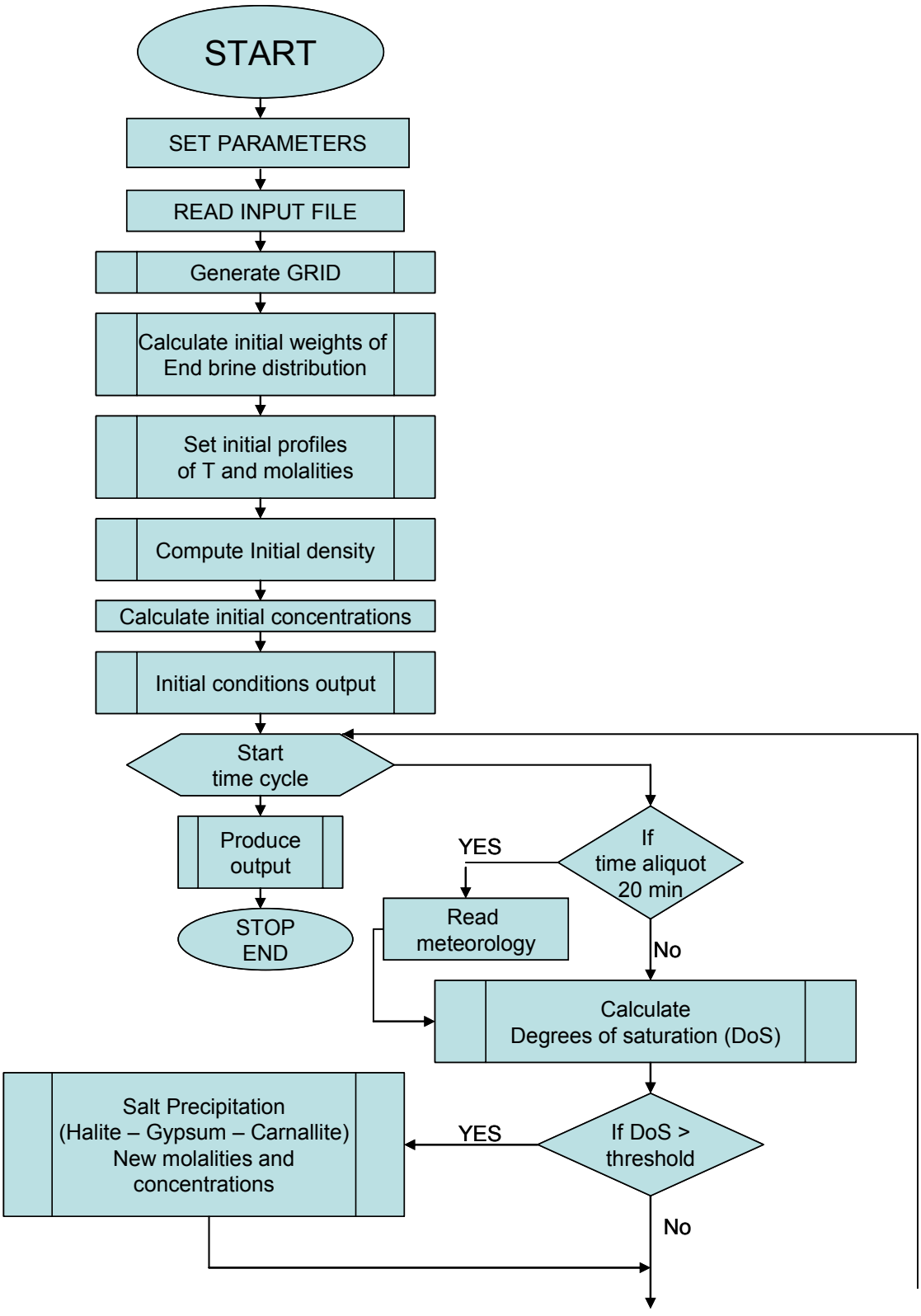

Figure 1.1 Flow chart of the 1D-DS-POM

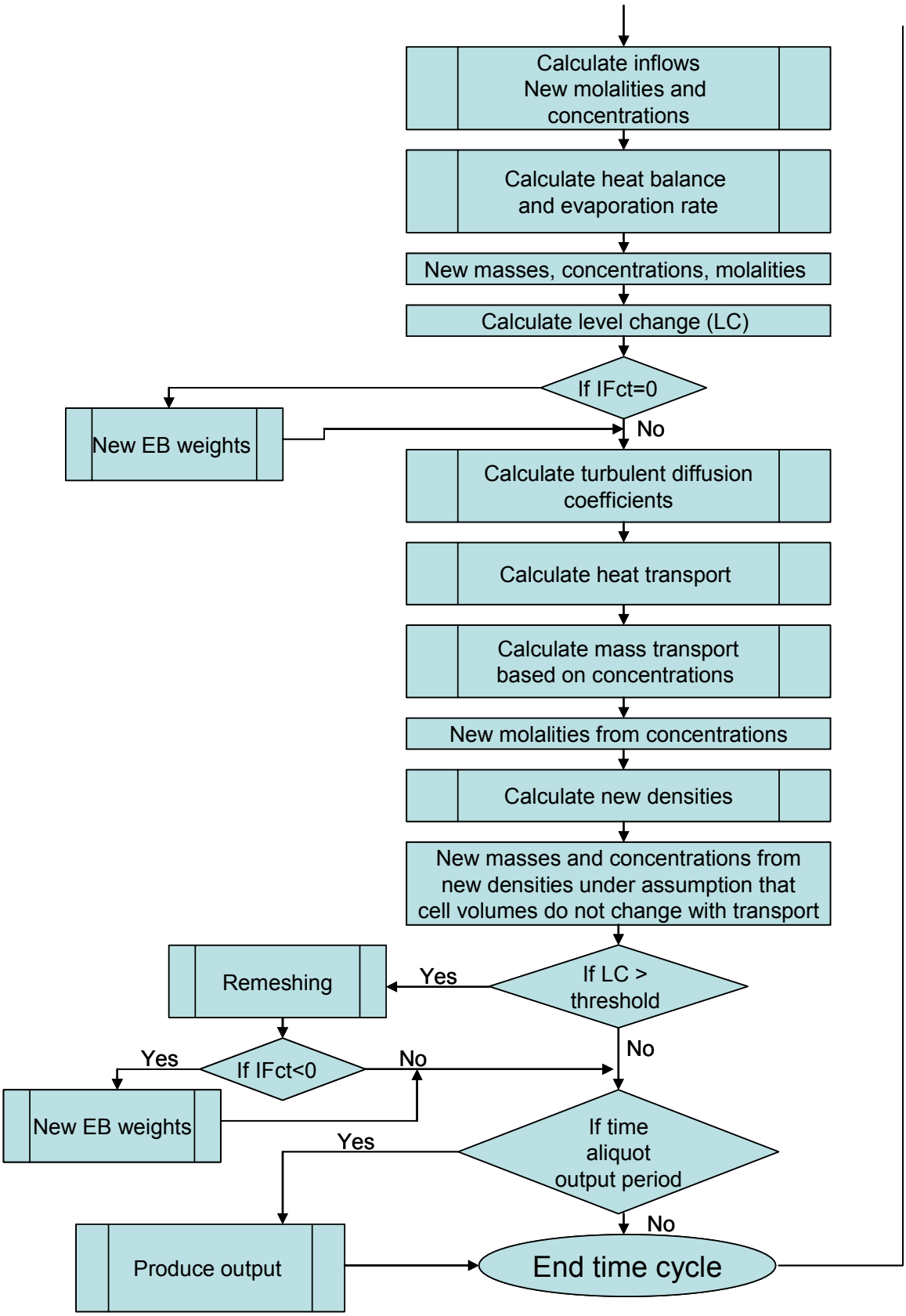

Figure 1.1 (cont.)

2 Physical Processes and Balances

2.1 Heat Exchange

The parameters for the heat exchange of the Dead Sea (DS) and its calibration are outlined in details in Lensky et al. (2005). These parameters have been incorporated into the 1D-DS-POM and are the basis for the calculation of heat exchange. The input for these calculations is the data collected every 20 minutes on the meteorological buoy on the Dead Sea. Following is a short description of these parameters and how they are derived from the input data, as coded in 1D-DS-POM. A more detailed description can be found in Lensky et al (2005) and references therein.

- *Incoming short wave (SW) radiation.* The net SW radiation that enters the DS is the incident SW radiation multiplied by albedo. The incident SW is measured directly on the meteorological buoy. Commonly, albedo over water bodies is in the range of 0.92 – 0.96. Following Lensky et al. (2005), the value assigned for albedo of the DS is 0.94.
- *Incoming and outgoing long wave (LW) radiation.* The net LW radiation is calculated as

$$LW=\varepsilon K_B(9.36\cdot10^{-6}\cdot T_a^{\,6} - T_S^{\,4}), \qquad (2.1.1)$$

  where:
  ε – the emissivity of the water body, ε=0.97;
  K_B– the Boltzmann constant, K_B=5.67·10-8 $Wm^{-2}K^{-4}$;
  T_a and T_S: air and sea surface temperature (SST), respectively (in ^oK). Whereas air temperature is an input meteorological data, SST is calculated by the model.
  At this stage the cloud cover is not accounted for, because it is generally low over the Dead Sea and precise observations are not available. We are currently collecting data through remote sensing and direct measurement of outgoing long wave radiation to calibrate it against the incoming short wave radiation. This will be incorporated in the next version of the code.
- *Heat of evaporation (EH).* The heat of evaporation is calculated as

$$EH=(a_{H2O}\cdot e_S - RH\cdot e_a)\cdot WF, \qquad (2.1.2)$$

  where:
  a_{H2O}: the activity of water in the brine (1.0 in freshwater, about 0.67 in the DS brine). Water activity is calculated by the model based on the instantaneous temperature and brine composition using the Pitzer thermodynamic approach (see sections 3.2 and 3.3).
  e_S and e_a: the saturated water pressure at SST and at the ambient air temperature, respectively, in mbar.
  RH: the relative humidity in the air (a fraction between 0 and 1), measured by the meteorological buoy.

  The saturated vapor pressure for a given air or sea surface temperature T is calculated as:

$$e=6.105\cdot\exp\{17.27\cdot T/(T+237.7)\}, \qquad (2.1.3)$$

  where e is in mbar and T – in ^oC.

  WF: wind function is calculated from the wind intensity:

$$WF=a+b\cdot WI^c \qquad (2.1.4)$$

where: WI is wind intensity ($m\ s^{-1}$) at 2 *m* above the sea surface; *a*, *b*, *c* are empirical coefficients.

Since in the future we intend to compare 1D-DS-POM runs with 2-D simulations based on the CE-QUAL-W2 code (Cole and Wells, 2006), we adopted the default values of CE-QUAL-W2, translated from mmHg to mbar: *a*=6.9, *b*=0.345, *c*=2. However, very preliminary calibration runs of 1D-DS-POM reveal that the values in the above wind function should be roughly reduced by a factor of 0.8. Thus, the model runs presented in this report are based on the following: *a*=5.5, *b*=0.28, *c*=2. Future calibration of the code will likely change these values.

- *Sensible heat exchange (H_S).* The amount of sensible heat is calculated using the Bowen approach:

$$H_S = C_B \cdot WF \cdot (T_S - T_a), \tag{2.1.5}$$

where:
C_B=0.61 is the Bowen constant,
T_S and Ta - sea surface and air temperatures, respectively.

2.2 Heat and Mass Transport

The model accounts for two different mechanisms of heat and mass transport: a) conductive-diffusive transport expressed through Fourier and Fick laws and b) turbulent mixing. Following Mellor-Yamada (1982), (the closure used in POM) the turbulent transport is calculated using the transport coefficients for heat ($\boldsymbol{K}_H$) and mass ($\boldsymbol{K}_M$):

$$\boldsymbol{K}_M = q \cdot L \cdot \boldsymbol{S}_M; \tag{2.2.1a}$$

$$\boldsymbol{K}_H = q \cdot L \cdot \boldsymbol{S}_H \tag{2.2.1b}$$

where q^2 is the turbulent kinetic energy and L is the turbulent length scale. The stability factors ($\boldsymbol{S}_H$, $\boldsymbol{S}_M$) are functions of the Richardson number, *Ri*, which is a measure of the relative importance of mechanical mixing and density gradient in the water column (ρ – density, *g* – acceleration due to gravity):

$$Ri = \frac{L^2}{q^2} \frac{g}{\rho} \frac{\partial \rho}{\partial z} \tag{2.2.2}$$

The Richardson number defined above is always considered negative. A positive *Ri* indicates unstable density gradients with active convective overturning. When *Ri* is large (typically considered above -1/4), then velocity shear is considered sufficient to overcome the tendency of a stratified fluid to remain stratified, and some mixing will occur. When *Ri* is small, turbulent mixing across the stratification is generally suppressed. Figure 2.2.1 presents the calculated stability factors as functions of the Richardson number.

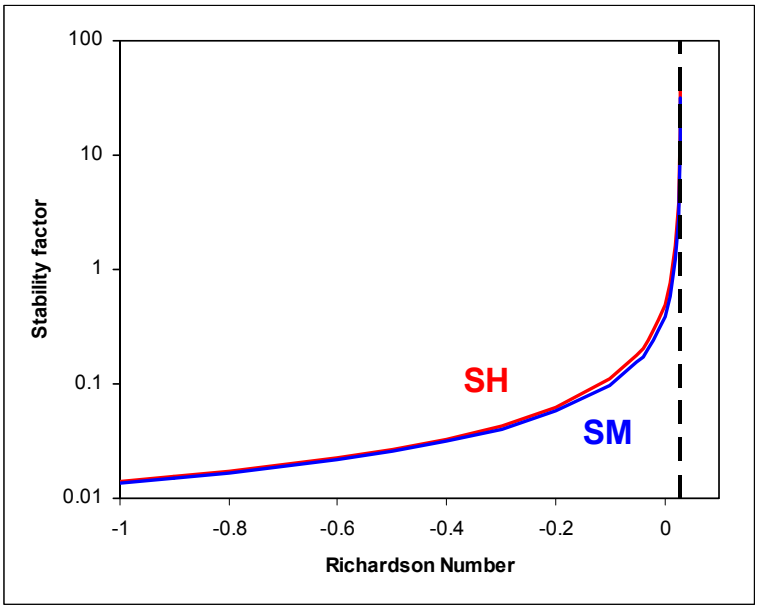

Figure 2.2.1. The stability factors as functions of the Richardson number.

Steady winds blowing on the sea surface produce a thin, horizontal boundary layer, the Ekman layer, with current velocity decreasing exponentially with depth. In line with the Ekman solution, and instead of following other 1D models and formulating complex empirical formulation for the decay of the turbulent kinetic energy with depth, we suggest the simplest parameterization which assumes exponential decay as a first approximation:

$$q^2 = A \cdot \exp\left(-\frac{z}{H}\right), \qquad (2.2.3)$$

The two adjustable parameters, A and H, correspond to the wind drag and depth of the Ekman layer, respectively. The current uncalibrated version uses A=0.01 (m/sec)^2 and H=2.5m. The latter value falls in the expected range of the Ekman layer depths which leads to thermocline depth of 25-30 m, in agreement with the observations. For the mathematical simplicity we also ignore possible depth dependence of the turbulent length scale and assume L=1m.

It should be noted that the above mechanisms of heat and mass transport incorporated in the code do not consider double-diffusive fluxes across sharp interfaces. However, the code allows calculating the stability ratio controlling the onset of the double-diffusive mixing. The double-diffusive fluxes across marginally stable interfaces (in terms of Richardson number) might be important and impact the timing of the overturn. These fluxes will be incorporated into the next version of the model and their importance will be examined during the model calibration.

2.3 Mass conservation

The density of seawater commonly range between 1,024 kg/m^3 and 1,030 kg/m^3, whereas the density of freshwater lakes does not deviate much from 1,000 kg/m^3. These small density differences allow to approximate mass conservation through the assumption of volume conservation, ignoring thermal expansion and volume change due to mixing. Such oceanographic and limnological models thus treat the water bodies as incompressible. In contrast, the huge density range in the Dead Sea system,

from 1,000 kg/m^3 in fresh water up to 1,350 kg/m^3 in the industrial end brines, calls for re-evaluation of this incompressibility assumption. In order to do so, 1D-DS-POM fully implements the mass conservation law (instead of the volume conservation assumption), thereby accounting for the compressibility of the system. This is done by tracking volume changes imposed by changes in densities related to mixing of different constituents, and to thermal expansion.

Mass balance consideration dictates that:

$$\frac{dM}{dt} = Q, \qquad (2.3.1)$$

Where M is the mass of a given volume (e.g., a numerical cell), Q is the rate of mass exchange with an external source or sink (e.g. inflows, evaporation, salt precipitation). Using $M = \rho \cdot V$ with density (ρ) being a function of temperature and composition (see section 3.2) the rate of volume change is:

$$\frac{dV}{dt} = \frac{Q}{\rho} - V\frac{1}{\rho}\frac{d\rho}{dt}, \qquad (2.3.2)$$

Equation (2.3.2) describes the volume change related to external sources or sinks of mass, and due to density change following changes in temperature and composition. Incompressible models reduce Eq. (2.3.2) by ignoring the second term on the right hand side which accounts for the density-related volume change. However, in 1D-DS-POM, Eq. (2.3.2) is incorporated in its complete form, thereby accounting for the compressibility of the Dead Sea brine and its mixtures.

2.4 Inflows and Pumping

Various inflows discharge into the DS, each characterized by different composition, temperature and flux, including pumping and discharge of brines by the chemical industries. The geographic locations of discharge (or pumping) points play no role in any 1D model. Yet, the depth at which the water enters the lake must be specified. Following is a list of inflows included in 1D-DS-POM. Their compositions are specified in the code, while their inflow flux is included in the input file:

- Freshwater inflows. This inflow includes, in addition to base flow from springs and Wadis surrounding the DS also direct precipitation and flash-floods. Given the hypersaline nature of the DS brine and its total mass, the salt flux into the lake from this source is negligible. Thus, freshwater inflow in the model is assumed to carry no chemical constituents, i.e. the water is regarded as de-ionized. Such water therefore only dilutes the cell to which it enters. Following Lensky et al. (2005) subsurface inflows to the DS is negligible and its volume is included in this freshwater inflow.
- Pumping of DS brine by the chemical industries. Withdrawal of DS brine from the lake includes also salt withdrawal. The brine that is withdrawn is assigned the chemical composition of the cell from which the water is pumped. Currently the industries pump their brines from the surface water and thus under current conditions the model pumps from the surface cell. Once seawater will be discharged to the lake the industries will most likely pump brines from the concentrated lower water body. The depth, and thus cell, from which pumping is done is an input parameter which can be changed in the run every year, at the beginning of the year.

- End brines (EB) discharge: After evaporation and salt precipitation in the evaporation ponds, the brines that are returned to the DS are significantly enriched in Ca, Mg, Cl and Br and depleted in Na, K, SO_4. Because the end brine is significantly denser than DS brine, upon entrance to the lake they tend, apart from mixing, also to sink and flow on the lake floor. In the model the EB flux may be introduced into any group of consecutive cells. This group of cells may be changed in the input file at the beginning of each year.
- Seawater (SW) inflows: Since SW is significantly less dense than DS brine (1,030 vs. 1,024 Kg m^{-3}) they are discharged into the surface cell of 1D-DS-POM.
- Reject brine (RB) from desalinization. The RB from the desalinization plant, which is part of the proposed Red Sea Dead Sea project, will be discharged to the DS. The common efficiency of such SW desalinization plant is around 50%, implying that the salinity of the reject brine is about twice that of SW. Thus, even though the RB is denser than SW, it is still significantly less dense than DS brine. Accordingly, 1D-DS-POM mixes the RB into the surface cell. The salt load and composition of the RB will be a function of the desalinization efficiency.

All inflows change the size, temperature and the concentrations of the dissolved ions of the cell to which they enter. Exception to this is pumping, which obviously only changes the cell size (and thus the overall DS mass and level), but does not affect ion concentrations and the temperature of the brine. Accordingly, Eq. (2.3.2) is applied at each time step for every cell, thus accounting not only for level change caused by a cell mass change, but also for level change caused by density changes. The change in Dead Sea level due to the inflows and pumping is the sum of all the changes in cells' sizes.

The new temperature of the cell is calculated as follows:

$$T_{new} = (T_{old} \cdot M_{old} + T_{in} \cdot M_{in})/M_{new} \qquad (2.4.1)$$

where T_{new}, T_{old} and T_{in} are the new temperature of the cell, its previous temperature and the inflow temperature, respectively, and M_{in} and M_{new} are the relevant masses of water. This calculation neglects possible differences in the specific heat of the various waters and brines involved in the calculation and the heat of their mixing.

The new composition of each cell is calculated from the ratio of the new mass of a given constituent (ion) to the new mass of H_2O (for molal concentration), and to the new mass of the cell (for g/Kg concentrations).

It should be noted that the present version of the code pumps from, and introduces water into a predetermined cell or group of cells. The model does not consider differential withdrawal as a function of distance from the specified cell. This process will be introduced in a future version, and its importance in determining the mixing across the thermocline and halocline will be examined.

3 Thermodynamics and Chemical Processes

The 1D-DS-POM code includes thermodynamic modules that are based on the Pitzer approach for hypersaline brines (Pitzer 1991) and adopted by Krumgalz for the Dead Sea brine system (Krumgalz 2001, Krumgalz and Millero, 1982). These modules are used for the determination of the density of the brine as a function of its instantaneous chemical composition and temperature, and for the precipitation of salts upon attainment of oversaturation.

3.1 Units Conversions

While the heat and mass transport equations are based on concentrations in salinity units [(g of ion)/(Kg of solution)], thermodynamic calculations, which determine the brine's degree of saturation with respect to different salts (e.g. halite, NaCl, or gypsum, $CaSO_4 \cdot 2H_2O$) and the amount of salt that needs to be precipitated to attain saturation, are based on molality units [mole/(Kg H_2O)]. In 1D-DS-POM, which is a multi-(chemical) component model we no longer follow the salinity of the brine but the individual concentration of the ions in salinity units. The model must therefore include modules that enable conversion back and forth between these units.

3.1.1 Molality to Salinity

Let m be the molal concentration [mole/(Kg H_2O)] of a dissolved ion or salt with the corresponding atomic or molecular weight μ.

If in 1Kg of H_2O there are $m \cdot \mu$ grams of the dissolved salt and no other salt is dissolved, then the weight of the solution is $(1000 + m \cdot \mu)$ grams. Accordingly, if in $(1000 + m \cdot \mu)$ grams of solution there are $m \cdot \mu$ grams of this salt, then the concentration of the salt, in salinity units (S; g/Kg Solution) is:

$$S = \frac{m\mu}{1000 + m\mu} \cdot 1000 \qquad (3.1.1)$$

Similarly, if the solution contains N ions, then the concentration, in salinity units, of the individual ions, i, is:

$$S_i = \frac{m_i \mu_i}{1000 + \sum_{i=1}^{N} m_i \mu_i} \cdot 1000 \qquad (3.1.2)$$

and the salinity of the solution is: $S = \sum_{i=1}^{N} S_i$

3.1.2 Salinity to Molality

Let S be the salinity in *g/Kg* Solution. Thus, there are S grams of salts for 1000-S grams of water. Accordingly, for 1000 grams of water there are x grams of salts:

$$x = \frac{1000 \cdot S}{1000 - S} \qquad (3.1.3)$$

assuming the salinity is derived from a single salt, then the molal concentration (m) of this salt is:

$$m = \frac{x}{\mu} = \frac{S}{\mu} \cdot \frac{1000 \cdot S}{1000 - S} \qquad (3.1.4)$$

Similarly, translating the concentration of the individual ions from salinity units (S_i) to molal units (m_i) is carried out as follows (S being total salinity, $S = \sum_{i=1}^{N} S_i$):

$$m_i = \frac{1000 \cdot S_i / \mu_i}{1000 - S} \qquad (3.1.5)$$

3.2 Equation of State

Commonly an equation of state (EoS) for a solution correlates its density with its temperature and salinity. The EoS for seawater, which is applied in oceanographic models, is valid over a small range of salinities and compositions typical for oceanographic process. The most recent EoS for the DS was established by Anati (1997), and is no exception to this approach. In fact, Anati notes that his equation will have to be re-evaluated every few years as the composition of the brine changes due to halite precipitation.

The densities that 1D-DS-POM needs to determine span beyond the mixing between DS (ρ~1,240 Kg m^{-3}) and seawater (ρ<1,040 Kg m^{-3}). It should account for densities as low as those of freshwater to the highly concentrated (up to 370 g/Kg) and hot (42°C) end brines that are discharged to the lake by the chemical industries. In addition, evaporation from the mixtures and the consequent increased concentrations, as well as changes in composition due to gypsum and halite precipitation must also be accounted for. Finally, the model should account for the evolution of the lake over the coming decades also if no seawater inflow is introduced. Under this scenario the DS density is expected to rise beyond its current value, while the composition of the lake will continue to change as halite precipitates from the brine.

To calculate the densities included in the range of composition described above we adopted the approach described by Krumgalz and Millero, (1982). This approach makes use of the Pitzer equations for the calculations of the thermodynamic properties of hypersaline brines and is based on the composition of the brine given in molality units.

The density of a solution at a given temperature and composition is calculated from Krumgalz et al., (2000) Eq. (24):

$$\rho_{mix} = \frac{1000 + \sum_{i=1}^{N} m_i \mu_i}{\frac{1000}{\rho_0} + \sum_{i=1}^{N} m_i \overline{V}_i^{\,0} + V_{mix}^{ex}} \qquad (3.2.1)$$

where:
m_i; concentration of ion i in molality (mol/kg H_2O);
μ_i: atomic weight of ion i;
ρ_0 : density of pure water at the given temperature (Eq. 15, Krumgalz et al., (2000));
$\overline{V}_i^{\,0}$: single-ion limiting partial molal volume (i.e. ionic partial volume at infinite dilution)
V_{mix}^{ex} : excess molal volume of a multiple-solute electrolyte solution.

There are two unknown functions in Eq. (3.2.1), $\overline{V}_i^{\,0}$ and V_{mix}^{ex}. The former is calculated from the data provided in Table 2 and Eq. (18) of Krumgalz et al., (2000). The calculations are based on the equation for thermal dependency of the limiting partial molal volume of Cl^- (Krumgalz, personal communication). The latter, V_{mix}^{ex}, is described by Eq. (8) in Krumgalz, (1995):

$$V_{mix}^{ex} = A_V \left(\frac{I}{b}\right) \ln\left(1 + b\sqrt{I}\right) + RT \left\{ 2 \sum_c \sum_a m_c m_a \left[B_{c,a}^V + \left(\sum_c m_c z_c \right) C_{c,a}^V \right] \right\}$$
$$+ RT \left[\sum_c \sum_{c'} m_c m_{c'} \left(2\Theta_{c,c'}^V + \sum_a m_a \Psi_{c,c',a}^V \right) + \sum_a \sum_{a'} m_a m_{a'} \left(2\Theta_{a,a'}^V + \sum_c m_c \Psi_{a,a',c}^V \right) \right]$$
(3.2.2)

where:
A_V (the Debye-Hückel slope) is given by Eq. (16), Krumgalz et al., (2000);
I - the ionic strength of the solution:

$$I = \frac{1}{2} \sum_{i=1}^{N} m_i z_i^2 \qquad (3.2.3)$$

z_i – ionic charge of ion i (a dimensionless integer*);*
b – a numeric coefficient*,* b=1.2 $kg^{1/2}$ $mol^{-1/2}$ *;*
$B_{c,a}^V$ is calculated in Eq. (7) of Krumgalz et al., (2000):

$$B_{c,a}^V = \beta_{c,a}^{(0)V} + \beta_{c,a}^{(1)V} g\left(\alpha_1 \sqrt{I}\right) + \beta_{c,a}^{(2)V} g\left(\alpha_2 \sqrt{I}\right) \qquad (3.2.4)$$

where:
$\beta_{c,a}^{(j)V}, j = 0-2$ are coefficients whose dependencies on temperature for different salts are presented in Krumgalz et al., (2000), Tables 4-6, and

$$g\left(\alpha_j \sqrt{I}\right) = \frac{2}{\left(\alpha_j \sqrt{I}\right)^2} \left[1 - \left(1 + \alpha_j \sqrt{I}\right) \exp\left(-\alpha_j \sqrt{I}\right)\right] \qquad (3.2.5)$$

(Krumgalz, 1995, Eq. 13). The coefficient α_1 = 2.0 for 1:1, 1:2 and 2:1 electrolytes and α_2 = 1.4 for 2:2 electrolytes; the parameter $\beta_{c,a}^{(2)V}$ is introduced only in the equations for 2:2 electrolytes. The temperature dependence of $C_{c,a}^V$ for different salts is given in Table 7 of Krumgalz, 2001.

The third term of Eq. (3.2.2) above consists of two terms that describe binary mixtures with a common ion. Of all the parameters that describe such interactions, only two are known (Krumgalz et al, 1995, Table IV) so the second part of Eq. (3.2.2) above reduces to:

$$RT \cdot m_{Na} m_K (2 \cdot 1.52E\text{-}05 - 6.72E\text{-}06\, m_{Cl}). \qquad (3.2.6)$$

This completes the description of the term V_{mix}^{ex}.

3.3 Degree of Saturation

1D-DS-POM determines the degree of saturation (DoS, Ω) and "precipitates" 3 salts from the brine: halite (NaCl), gypsum ($CaSO_4 \cdot 2H_2O$) and carnallite ($KMgCl_3 \cdot 6H_2O$). Salt precipitation occurs when the brine is oversaturated with respect to that particular salt.

The degree of saturation (Ω) of salt $A_\alpha B_ß \cdot nH_2O$ is defined as:

$$\Omega_{A_\alpha B_\beta \cdot nH_2O} = \frac{(m_A \gamma_A)^\alpha (m_B \gamma_B)^\beta a_{H_2O}}{K_{SP}} \qquad (3.3.1)$$

where:

A and B are the cation(s) and anion(s) making up the salt, respectively,
m: molality of the corresponding component/ion,
γ: ion activity coefficient,
a_{H2O}: water activity in the brine
K_{SP}: thermodynamic solubility product. The latter depends on temperature but not on the brine composition.

In 1D-DS-POM, determination of DoS is carried out in a newly written thermodynamic module which is based on the Pitzer approach, adopted for the Dead Sea by Krumgalz (2001). This approach allows determining the ion activity coefficients, γ, in solutions of high ionic strengths.

3.4 Salt Precipitation

1D-DS-POM accounts for salt precipitation through two actions: a) stoichiometric decrease in the concentration of the ions making up the salts so that the brine will re-attain saturation. In case this decrease also involves changes in the concentration of the rest of the chemical constituents (when the precipitated salt includes water molecules), the concentration of all ions is computed (see below). b) Recording of the amount of salt that precipitated. This value is then translated into the thickness of salt that accumulates and raises the lake floor and thus impacts the water level.

At present the code ignores kinetic effects and considers only equilibrium thermodynamics. Theoretically, salts should precipitate when the degree of saturation, Ω, exceeds saturation, i.e. $\Omega > \Omega_{sat}=1$, and cease once saturation is regained (i.e. at $\Omega = \Omega_{sat} =1$). However, because of numerical reasons 1D-DS-POM begins precipitating salts only when a small predetermined oversaturation is attained. We define this excess oversaturation, ε, as the threshold beyond which salt begins to precipitate. ε is an input parameter which in all runs is in the range of 10^{-6} to 10^{-4}. It is also possible to numerically increase (or decrease) Ω_{sat} to any value, Ω^0_{sat}, so that salt begins – and stops – precipitating at higher (lower) Ω, to account for kinetic effects. For example, the Dead Sea is known to be oversaturated with respect to gypsum. In order to account for this, Ω^{gypsum}_{sat} (=1) is replaced by $\Omega^{0,gypsum}_{sat}$. Precipitation then will start when $\Omega^{gypsum} > \Omega^{0,gypsum}_{sat} + \varepsilon$, and stop when Ω regains value less than, or equal to $\Omega^{0,gypsum}_{sat}$, i.e $\Omega \leq \Omega^{0,gypsum}_{sat}$.

The algorithm formulated in the 1D-DS-POM for salt precipitation is outlined below. Unlike other codes for salt precipitation, in which saturation is re-gained through a series of iterations of precipitation and recalculation of the DoS, the suggested algorithm precipitates salt through a single step, thereby minimizing calculation time.

Because of the short time steps in the model (see below), the code does not allow the brine to attain high oversaturation. Thus, the amount of precipitated salt at each time step is small. Under this constraint we assume a linear relation between the change in the DoS with respect to the change in the molal concentration of the corresponding salt (m_{salt}):

$$\frac{\partial \Omega}{\partial m_{salt}} = \frac{\Omega - \Omega_{sat}^{0}}{\Delta m_{salt}}, \qquad (3.4.1)$$

where for halite $\Delta m_{salt} = \Delta m_{Na} = \Delta m_{Cl}$ while for gypsum $\Delta m_{salt} = \Delta m_{SO4} = \Delta m_{Ca} = 1/2\, \Delta m_{H2O}$

The derivative $\left(\frac{\partial \Omega}{\partial m_{salt}} \right)$ is calculated numerically using incremental change in the molal concentration of the corresponding salt (m_{salt}). After establishing this derivative, the mass (Δm_{salt}) needed to be "precipitated" to attain saturation (Ω_{sat}^{0}) is calculated in a single step:

$$\Delta m_{salt} = \frac{\Omega - \Omega_{sat}^{0}}{\left(\frac{\partial \Omega}{\partial m_{salt}} \right)} \qquad (3.4.2)$$

When the precipitated salt is gypsum or carnallite, which are hydrated salts, their precipitation impacts the concentrations of all ions in solution. Thus, once the amount of salt that needs to be precipitated to attain saturation is established, the concentrations of the rest of the ions in solution are recalculated.

4 Numerical Method

The numerical algorithm uses a finite difference scheme with moving grid points and a fixed time step. All model variables are prescribed at the center of each cell, which is defined as the interval between adjacent grid points. Variable spacing between grid points allows high accuracy of calculations close to the surface, as discussed in section 4.1 below. The sensitivity of model results to time step is discussed in section 4.3.

The change in the size of cell number k, Δz_k, is calculated using equation (2.3.2) written in terms of finite difference

$$\Delta z_k = \frac{\Delta M_k}{\rho_k} + z_k \frac{\Delta \rho_k}{\rho_k}. \qquad (4.0.1)$$

where ΔM_k is the change in the mass of the brine in the cell; ρ_k and $\Delta \rho_k$ are the resulting density and the change in the density of the brine in the cell during a single time step, respectively, and z_k is the initial cell thickness. Tracking the change in the

cells' size, including changes related to density changes, ensures mass conservation and accounts for the compressibility of the system.

The run results described hereafter are model runs with meteorological input data of, unless otherwise stated, year 1998 (chosen due to the least amount of gaps in the data). Annual freshwater inflow volume is 350 million cubic meters (MCM/yr). The chemical industries pump 525 MCM/yr of DS brine and discharge 240 MCM/yr of end brines. When runs are carried out for more than a year, the 1998 input data are duplicated.

4.1 Grid Geometry

The 1D-DS-POM grid is composed of points which divide the water column into cells whose thickness is not uniform (Table 4.1.1). The topmost cells (down to 5 m depth), where most of the chemical and physical processes occur are thinnest. The following depth range (5-45 meter) includes the annual thermocline and halocline, which commonly develops at a depth of 25-30 meters, is also divided into relatively thin cells. This should enable attaining good resolution for the processes taking place at the transition layer between the lower and upper water bodies. The simulated thickness of this transition layer depends not only on the turbulent mixing, but also on the molecular diffusion and heat conduction. The high value of the molecular diffusion coefficient (10^{-5} m^2/s), adopted in the original POM, leads to stretching of the transition zone over several meters over period of several months. When considering a stable stratification that could last years (such as expected when seawater will be discharged), it would stretch the transition layer over tens of meters. To avoid this artifact related to unrealistically high molecular diffusion coefficient, we reduced it by three orders of magnitude (10^{-8} m^2/s). With this value the stretching of the transition zone is negligibly small even over time scale of years. On the other hand, this value is sufficiently high to eliminate grid size dependency as demonstrated below.

At depths of about 10-15 meters below the transition zone (45-95 m), the water column is about homogeneous and thus cells' thickness was increased, while the bottom cells are thickest. The last grid point is fixed at the sea floor, whose depth is set according to the normalized depth. The latter is defined as the depth corresponding to a rectangular basin whose area and volume equal those of the lake, at the given time. In Jan 1st 1998, when water level, surface area and brine volume were -410.8 meters, 655.0 km^2, and 137.6 km^3, respectively, the normalized depth was 210.0m.

Table 4.1.1: Depth distribution of the 1D-DS-POM grid (70 points).

Depth Range (m)	Cell thickness (m)	Number of cells
0-5	0.5	10
5-45	1	40
45-95	5	10
95-185	10	9

To verify that the model results do not depend on the grid construction, a 1 year run with 70 grid points (hereafter referred as “standard grid”) was compared to runs in

which the grid was either changed by doubling or about halving the number of grid points (i.e. 140 and 36 points, Tables 4.1.2 and 4.1.3, respectively). In addition the model was run with a grid that included 70 grid points that were spaced evenly, i.e. with a constant cell thickness of about 3.04m). In each case the last grid point (#140 for the fine grid, #36 for the coarse one and #70 for the equidistant grid) is always fixed at the normalized sea depth, which at the onset of the run is 210 m.

Table 4.1.2 Depth distribution of the fine grid (140 points)

Depth Range (m)	Cell thickness (m)	Number of cells
0-5	0.25	20
5-45	0.5	80
45-95	2.5	20
95-190	5.0	19

Table 4.1.3 Depth distribution of the coarse grid (36 points)

Depth Range (m)	Cell thickness (m)	Number of cells
0-5	1	5
5-45	2	20
45-95	10	5
95-195	20	4

All runs resulted in a similar SST (Fig. 4.1.1), surface salinity (Fig.4.1.2), density and the weight of precipitated salts throughout a one year run. The results of the run with 70 grid points are presented in Table 4.1.4. Table 4.1.5 presents the maximal and final differences between the runs. The maximal temperature and salinity differences, which last less than 12 hours, are caused by the slight difference in the timing of overturn of the water column. Figs 4.1.3 and 4.1.4 present the differences in the SST and salinity over one year runs. Note the fine scales of the graphs, which nevertheless include all differences except those which occur due to the slight difference in the timing of the overturn.

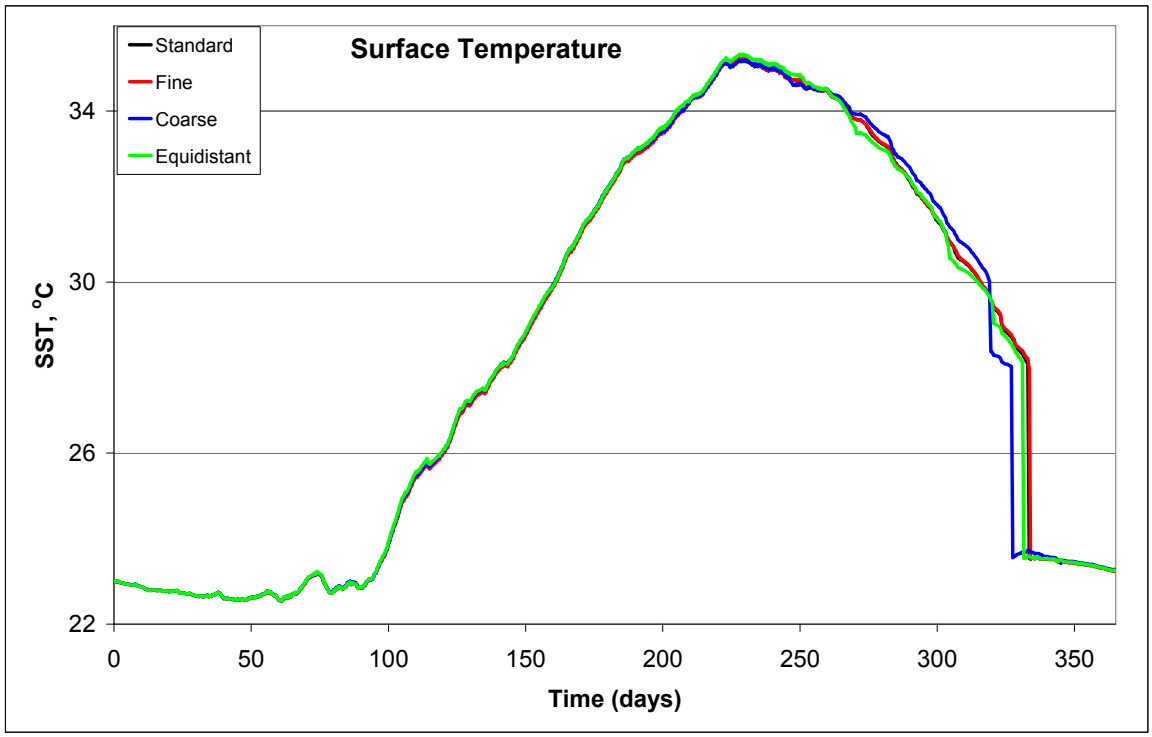

Figure 4.1.1. SST in one year runs with different grids.

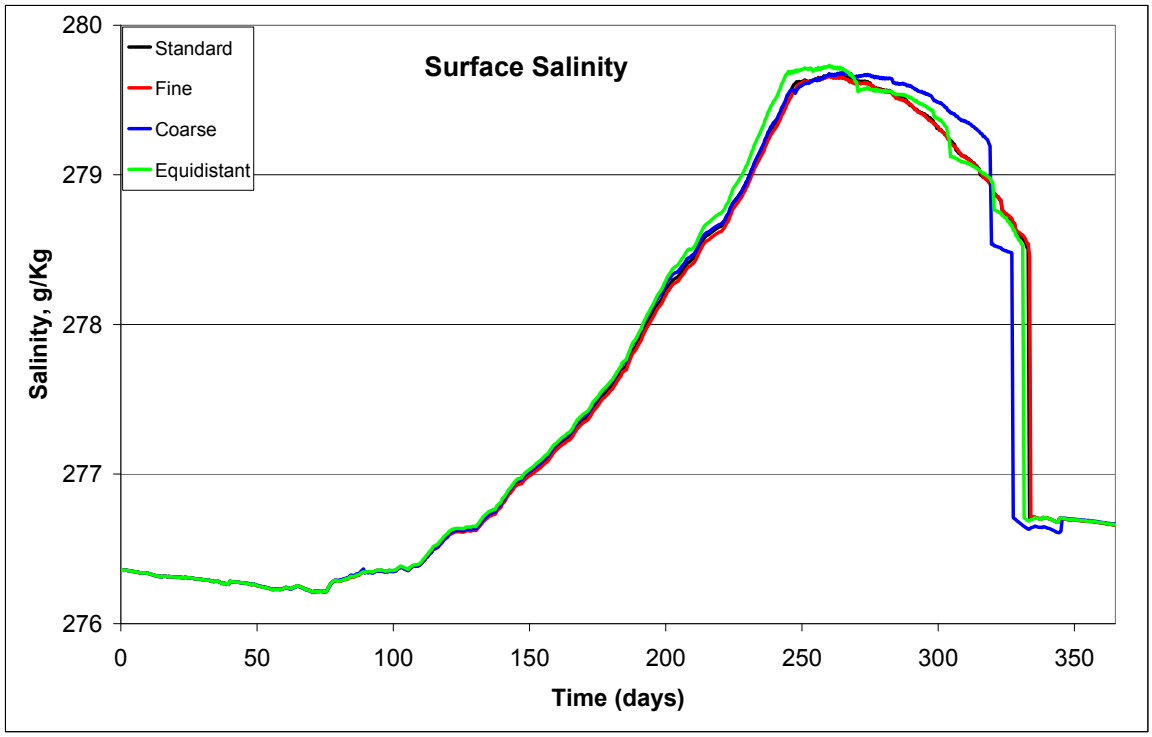

Figure 4.1.2. Sea surface salinity in one year runs with different grids. Note that the line of the run with the standard grid coincides with that of the fine grid.

Table 4.1.4 Results of the one-year run with 70-points grid.

Parameter	SST	Surface Salinity	Surface Density	Deposited Salt	Day of overturn
Value	23.24 °C	276.66 g/Kg	1238.21 Kg m^{-3}	$1.35 \cdot 10^{11}$ Kg	333.0

Table 4.1.5. Differences in run results between the fine grid (140 points) and standard 1D-DS-POM grid (70 points), between fine grid and the coarse grid (36 points) and between the fine grid and the equidistant grid (70 points). Note that the maximal temperature differences are due to slight differences in the timing of overturn (see last column). The number in parentheses is the maximal difference other than that caused by overturn.

Grids	ΔT, °C		ΔS, g/Kg		Δρ, Kg m^{-3}		Δ(D. salt), 10^8 Kg		Δ(Over-turn), days
	Max	Final	Max	Final	Max	Final	Max	Final	
Fine-standard	4.4 (0.09)	-0.003	1.7 (0.05)	$-5 \cdot 10^{-4}$	0.04	$9 \cdot 10^{-4}$	-10	0.7	0.5
Fine-Coarse	5.1 (1.2)	-0.03	2.0 (0.4)	-0.005	0.14	0.008	-62	18	6.5
Fine-Equi-distant	4.8 (0.4)	0.01	1.9 (0.2)	-0.002	0.15	0.003	-51	4.8	2.5

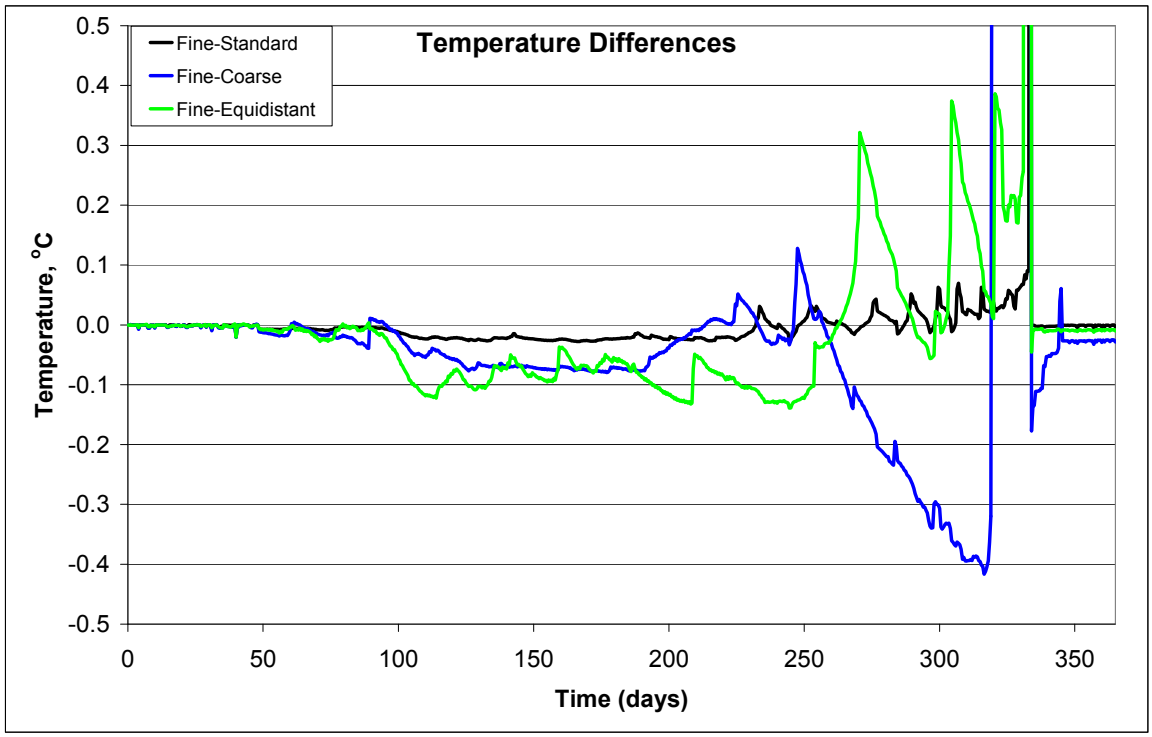

Figure 4.1.3. Temperature differences between one year runs with different grids. Note that the smallest differences are between the temperatures obtained with the fine and standard grids.

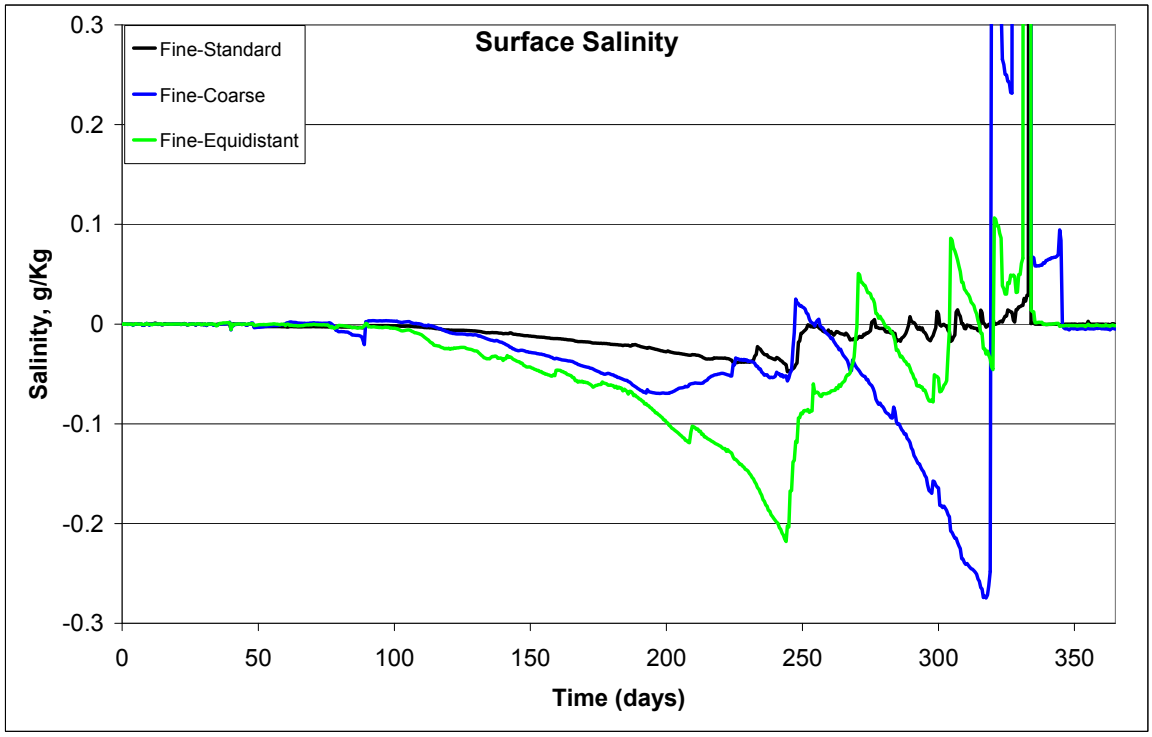

Figure 4.1.4. Salinity differences between one year runs with different grids. Note that the smallest differences are between the salinities obtained with the fine and standard grids. The salinity differences that exceed the scale are only those associated with the timing of the overturns.

These runs clearly shows that the choice of the 70 points grid for 1D-DS-POM is valid, and does not introduce errors in the model calculations.

The time of the run with fine grid is 2 times longer than the time of the run with standard grid. The small improvement of the numerical accuracy expected from the fine grid does not justify the longer runs. Hence, the 70 points grid is recommended for practical purposes.

4.1.1 Grid Remeshing

During simulation, the thickness of some cells change: the uppermost cell is affected by evaporation and freshwater inflow, whereas deeper cells change thickness due to temperature changes and processes related to the activities of the chemical industries. In the code the industries have the option to pump DS brine from the surface or from deeper cells. The end brines, which are discharged by the industry during the same time period that pumping is carried out, flow close to the seafloor while mixing with the DS brine above. Finally, salt precipitation, which may occur from the entire water column, impacts on cell size through mass change. All these processes deform the initial grid and may reduce numerical accuracy. Thus grid re-meshing and re-interpolation of the model variables is required throughout the simulation.

Dead Sea surface area changes throughout the run as water level rises or declines, requiring adjusting the normalized depth. This correction is introduced during the remeshing by recalculating the normalized depth, using the current surface area and volume.

It should be noted that remeshing is the only numerical process in the current version of the model that does not conserve mass. Benchmarking tests indicate that the latter has no impact on the overall accuracy of the results except for a negligible change in the mass: maximal change during a single remeshing is about $2 \cdot 10^{8}$ Kg or $1.4 \cdot 10^{-4}$ % of the total DS mass. The overall change of the mass due to the remeshing during a 1 year run with 1 meter level drop (26 remeshings) is on the order of 10^{-3} % (see section 5.3). Mass deficit due to remeshing as a function of time is presented in Fig. 4.1.5:

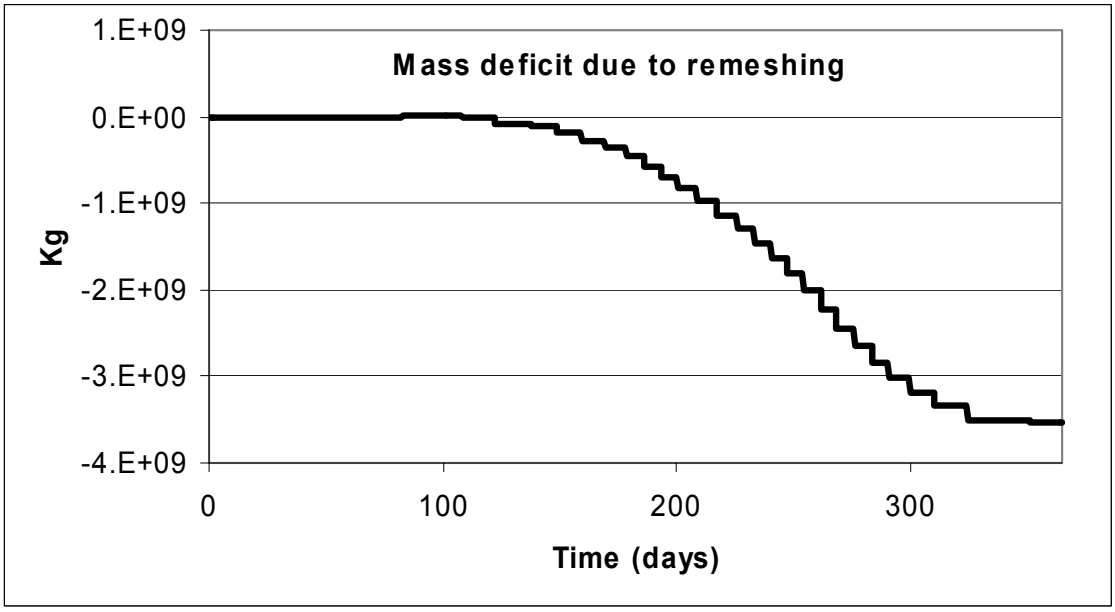

Figure 4.1.5 Mass deficit due to remeshing during a 1 year run with water level drop of 1 meter. Total mass of the DS is $1.7 \cdot 10^{14}$ Kg.

1D-DS-POM remeshes its grid when any one of the cells has changed its thickness by more than 10%. During remeshing, the cells re-attain their original thickness except for the five deepest cells. These five are assigned identical thicknesses that together adsorb the change in the overall depth of the water column. Remeshing is carried out for both water level rise and water level decline.

1. Remeshing following cell shrinking

A linear interpolation is used to compute the temperature and composition at each new grid point following the remeshing:

$$\xi_n(k) = \xi_o(k) + \frac{\xi_o(k+1) - \xi_o(k)}{z_o(k+1) - z_o(k)} \cdot \left(z_n(k) - z_o(k)\right),$$

where:
ξ_n – is a variable (e.g. temperature) after the remeshing,
ξ_0 – the same variable before remeshing,
k – grid point number,
z_0, z_n – the depth of the cell's upper grid point before and after the remeshing, respectively.

2. Remeshing following cell expansion

Remeshing following cells' expansion is carried out using the same notations as above, except that in this case it is possible to use the previously calculated point (k-1) to calculate point number k, which was not possible in the former case.

$$\xi_n(k) = \xi_o(k) + \frac{\xi_o(k-1) - \xi_o(k)}{z_o(k-1) - z_o(k)} \cdot \left(z_n(k) - z_o(k)\right)$$

4.2 Heat and Mass Transport

As in the original POM, vertical transport of temperature and individual ions (in g/Kg solution) is calculated using implicit-in-time finite-difference scheme, which eliminates time-step constraints for the spacing of the grid points and permits the use of fine vertical resolution close to the topmost grid points. The procedure is described in detail in POM Users Guide (Mellor, 2004). The boundary conditions for the turbulent heat and mass transport equations at the surface are heat flux (following the heat exchange described in section 2.1) and zero mass flux. The evaporative mass flux as well as inflows and outflows are accounted for by changes in the size of the corresponding grid cell, i.e. the uppermost cell for the evaporative flux and predefined cells for in and outflows. At the bottom, zero heat and mass flux boundary condition is adopted and thus all the remaining penetrative heat is absorbed in the lowermost cell.

4.3 Time Step Selection

The accuracy of model calculations increases with decreasing time step, but at a cost of increasing run time. In order to establish the optimal numerical time step for 1D-DS-POM, several runs were conducted with different time steps (5 sec, 5 min, 10 min and 20 min) at otherwise identical conditions and input parameters. All runs were conducted with the meteorological data from year 1998 and annual inflow volume of 350 MCM. The output parameters that were compared include: sea surface temperature (SST), sea surface salinity, sea surface density, the amount of precipitated salt, the amount of evaporated water and the change in water level. Two sets of runs were conducted: 1 year and 52 years runs. As outlined below, the optimal time step was found to be 10 minutes.

4.3.1 One year runs

Table 4.3.1 compares the final outputs of four one-year runs with different time steps. Since the run with the shortest time step (5 seconds) is assumed to have the most precise numerical results, the outputs of the other 3 runs are compared to its output. All runs were carried out on the same computer with a Pentium 4 processor (3GHz, 512 Mb RAM). The executables were compiled with Intel Visual Fortran compiler, Professional Edition for Windows, version 10.1.

Table 4.3.1. Comparison between the final outputs of four one-year runs with different time steps.

Time Step	5 sec	5 min	10 min	20 min
SST (°C)	23.237	23.235	23.236	23.238
Water Level (m above mean sea level)	-411.9461	-411.9465	-411.9461	-411.9455
Evaporation (m)	0.9975	0.9977	0.9976	0.9972
Surface Salinity (g/Kg)	276.661	276.659	276.659	276.660
Surface Density (Kg/m^3)	1238.2132	1238.2136	1238.2135	1238.2129
Precipitated salt (Kg)	$1.3508 \cdot 10^{11}$	$1.3523 \cdot 10^{11}$	$1.3514 \cdot 10^{11}$	$1.3489 \cdot 10^{11}$
Run time	52 min	1 min	36 sec	17 sec

Surface Temperature

The differences in SST during the year between the 5 sec run and the other runs are presented in Figure 4.3.1. The differences at all times do not exceed 0.04°. The differences between 5 sec and 10 min are generally less than 0.01° except during the overturn and the 10 min time step is thus considered optimal.

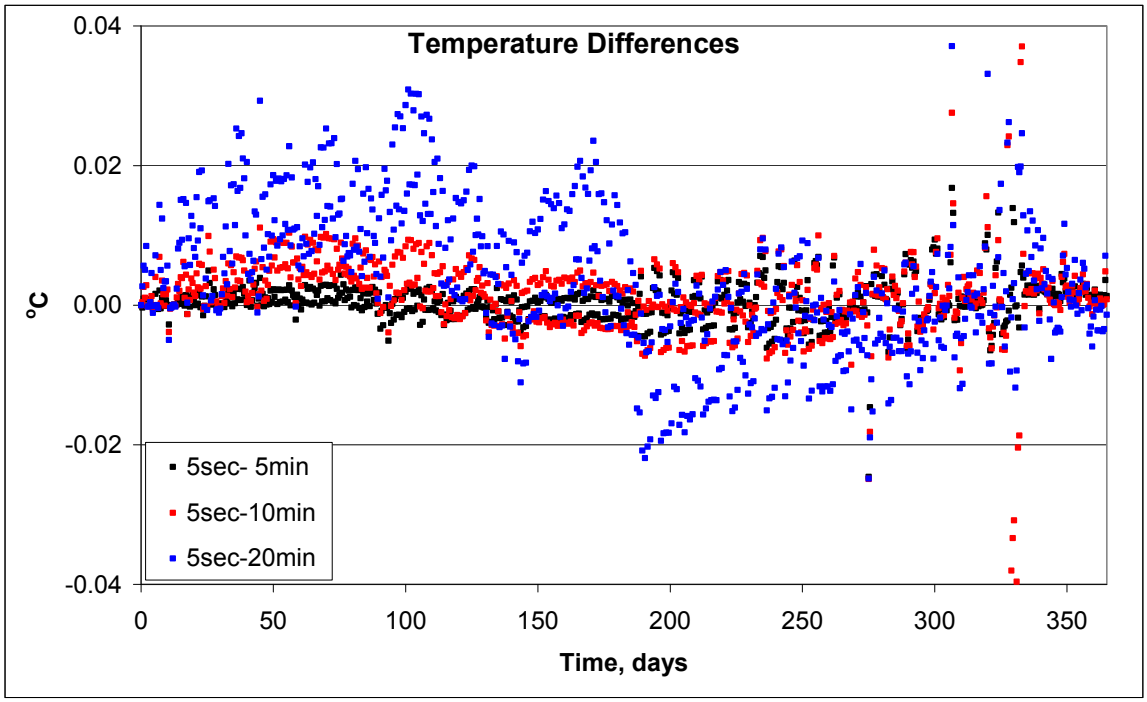

Figure 4.3.1. Temperature differences between the 5 sec run and: 5 min (black), 10 min (red) and 20 min (blue) runs.

Water level and evaporation

Water level and evaporation are only slightly affected by changes in time step. Compared with the 5 sec run, water level differences do not exceed 1.6 mm in the 20 min time step, 0.7 mm in 10 min time step and 0.4 mm for the 5 min time step runs. (Fig. 4.3.2). The deviation in evaporation of these former runs compared to the 5 sec run are 0.8 mm (0.09%) and 0.3mm (0.03%) and 0.2mm (0.02%), respectively (Fig. 4.3.3).

Surface salinity and density

Differences in sea surface salinity (Fig. 4.3.4) and density (Fig.4.3.5) between the four time step runs are negligible and do not exceed 0.02 g/Kg (0.008%,) and 0.02 kg m^{-3} (0.002%), respectively.

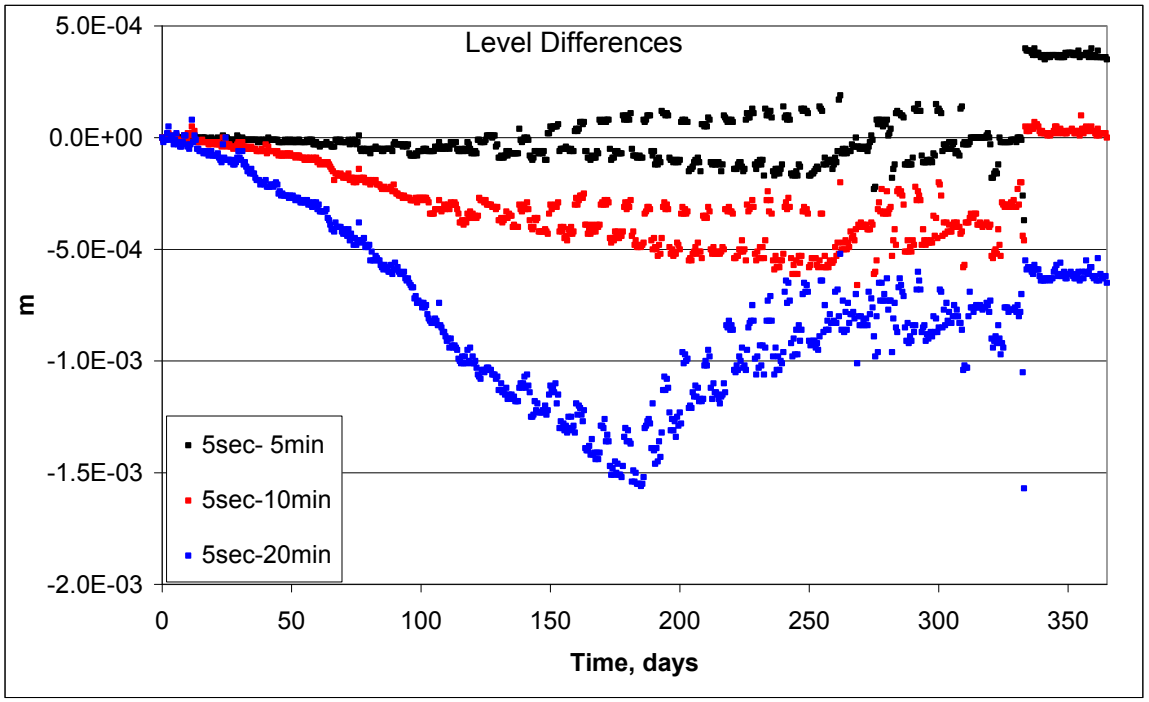

Figure 4.3.2. Comparison of level change between runs with different time steps. Note the small scale of the water level axis.

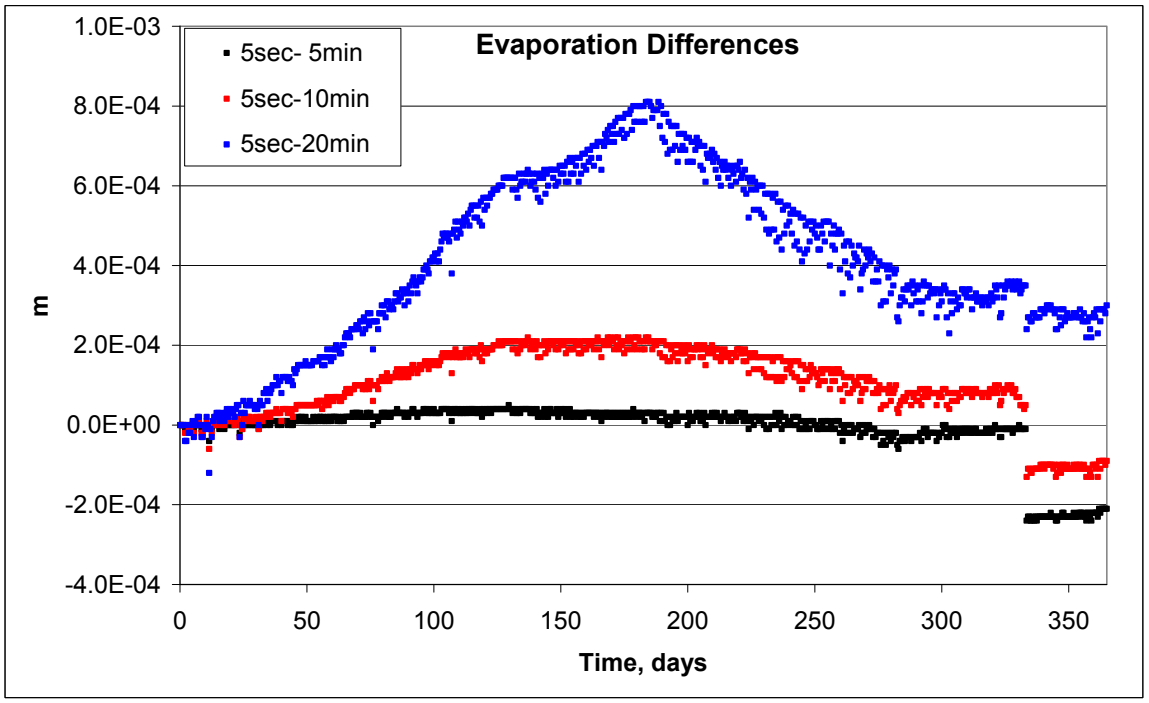

Figure 4.3.3. Comparison between evaporation in runs with different time steps.

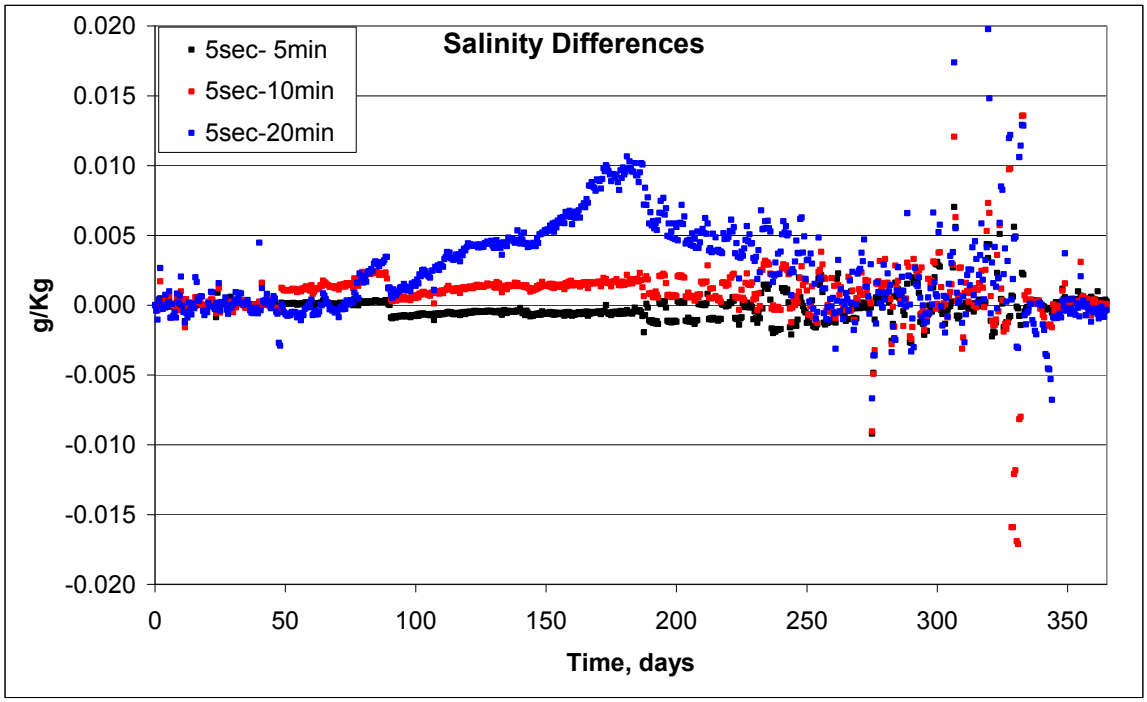

Figure 4.3.4. Comparison between surface salinities in runs with different time steps.

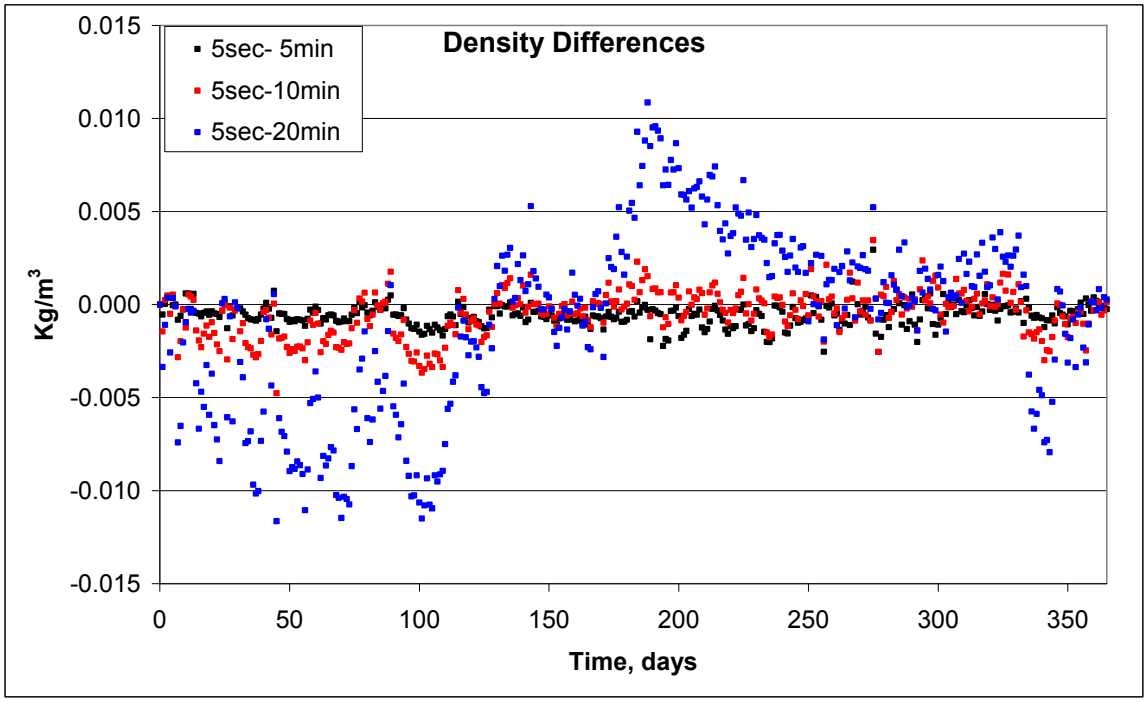

Figure 4.3.5. Comparison between surface densities in runs with different time steps.

Salt precipitation:

Differences between the accumulated precipitated salt are generally minor (Fig 4.3.6) and develop because of two main reasons: a) slight differences in SST between the runs which result in different degrees of saturation. b) 1D-DS-POM calculates the amount of precipitated salt based on the degree of saturation over the threshold. The actual nonlinear process is approximated by linear calculations based on the assumption that the oversaturation gained over the period of one time step is small

(see section 3.4). Thus, different time steps result in slightly different amounts of precipitated salt. The maximum difference between the runs is less than $6 \cdot 10^8$ Kg (0.4%), and by the end of the runs it is only $1.9 \cdot 10^8$ Kg (0.4%). As shown above, this has negligible impact on the salinity and density of the brine and on the final water level (which is determined also by the accumulation of salts at the seafloor).

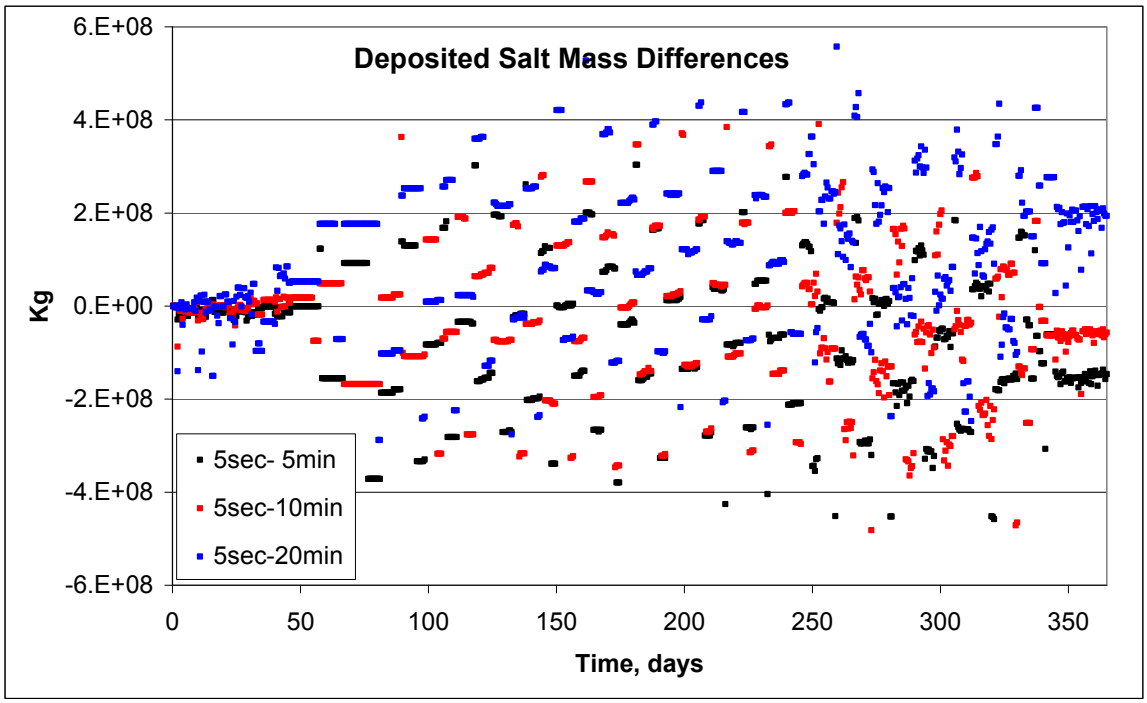

Figure 4.3.6. Comparison between the weights of precipitated salt in runs with different time steps. Thus the comparison of the results of 1-year long runs with different time steps suggests that the optimal time step for 1D-DS-POM is 10 minutes.

4.3.2 52 year runs

The 52 year runs with the four different time steps support the choice of 10 minutes as the optimal time step. Table 4.3.3 shows that the differences between the output variables at the end of 52 year runs are minimal.

Table 4.3.3. Comparison between the final outputs of the four 52-year runs with different time steps.

Time Step	5 sec	5 min	10 min	20 min
SST (°C)	25.079	25.081	25.082	25.118
Water Level (m above mean sea level)	-467.053	-467.050	-467.048	-467.039
Evaporation (m)	50.100	50.101	50.103	50.102
Surface Salinity (g/Kg)	293.802	293.804	293.807	293.816
Surface Density (Kg/m^3)	1259.726	1259.728	1259.731	1259.724
Precipitated salt (Kg)	$5.573 \cdot 10^{12}$	$5.574 \cdot 10^{12}$	$5.575 \cdot 10^{12}$	$5.574 \cdot 10^{12}$

It should be noted that during the runs, differences may reach higher values, e.g. up to several degrees in SST, but this always happens in conjunction to the timing of overturn; due to slight differences between runs, overturns occur at slightly different timings, resulting in temporal difference between the output variables.

To sum up, the optimal time step for 1D-DS-POM is 10 minutes.

5 Benchmarking

The behavior of the simulated system is very complex and can hardly be predicted using analytical solutions. However, some analytical solutions can be obtained for simplified conditions. Here we present comparisons between numerical and analytical results obtained for simplified conditions.

5.1 Heat Balance and Related Level Change

Under steady state conditions, the net heat flux should be zero, i.e. the incoming and outgoing heat fluxes should be identical. Given constant meteorological conditions, the equilibrium sea surface temperature (SST), T_{eq}, can be calculated analytically. These calculations are done by iterative procedure, which account for non-linear coupling between surface temperature and water activity. Thus, different values for water activity are obtained for every equilibrium temperature. In order to check the heat balance modules, the model was run under conditions that should lead to such a steady state temperature. This was done by switching off all processes that influence SST other than those associated directly with heat exchange. Thus, the following were set to be inactive: salt precipitation, inflows and level change following evaporation. Since the latter is part of the energy balance, the model continued to account for heat of evaporation even though water level was held constant.

Under the above conditions, when runs begin with a homogeneous water column of T_i such that $T_i>T_{eq}$, SST as well as the rest of the water column should cool to T_{eq} and the water column should shrink (see Eq.(2.3.2), second term). For $T_i<T_{eq}$, SST should rise to T_{eq}, thermal stratification should develop and water level should rise. For runs beginning with $T_i= T_{eq}$, SST, the temperature of the rest of the water column and the water level should not change.

The influence on T_{eq} of each of the meteorological input parameters, i.e., short wave radiation (SW), air temperature (T_a), relative humidity (RH), and wind intensity (WI) were checked individually. This was done by running a "base case" followed by runs in which a single meteorological parameter was changed at a time, leaving the others unchanged. Table 5.1.1 presents the input meteorological data for these benchmarking runs, along with the analytical T_{eq}. The last column in the Table refers to the Figure number which presents the model SST result for each set of data. Each Figure describes three runs with variable initial temperatures: $T_i>T_{eq}$, $T_i=T_{eq}$ and $T_i<T_{eq}$.

Table 5.1.1. Meteorological data for the benchmarking of heat exchange.

run	Incoming short wave radiation (W/m^2)	T Air (°C)	Relative humidity (%)	Wind intensity (m/s)	T_{eq} (°C)	Figure number
Base case	200	30	66	7.5	32.07	5.1.1
1	100	30	66	7.5	30.39	5.1.2
2	200	35	66	7.5	36.81	5.1.3
3	200	30	40	7.5	27.74	5.1.4
4	200	30	66	5.5	33.00	5.1.5

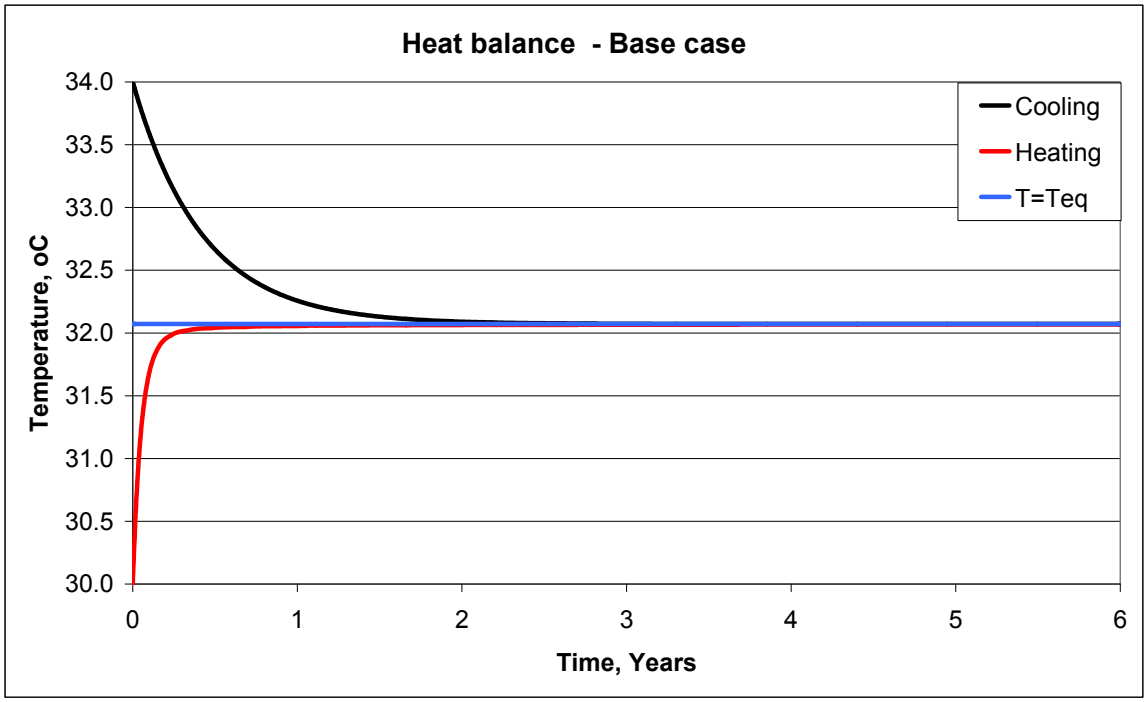

Figure 5.1.1. Model SST for the "base case" benchmarking of heat exchange (see Table 5.1.1, first row). Runs begin with a homogeneous water column at SST above, at and below the analytical steady state SST.

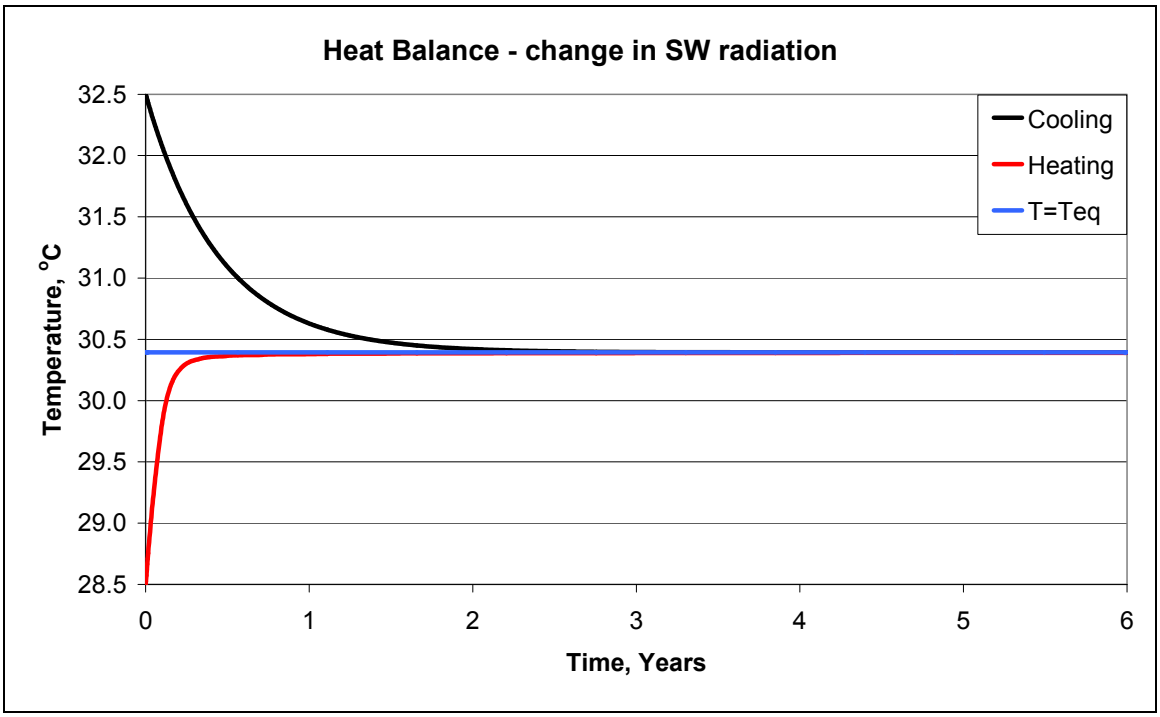

Figure 5.1.2. Model SST for input data with SW radiation that is lower than in the "base case" (see Table 5.1.1, run #1)

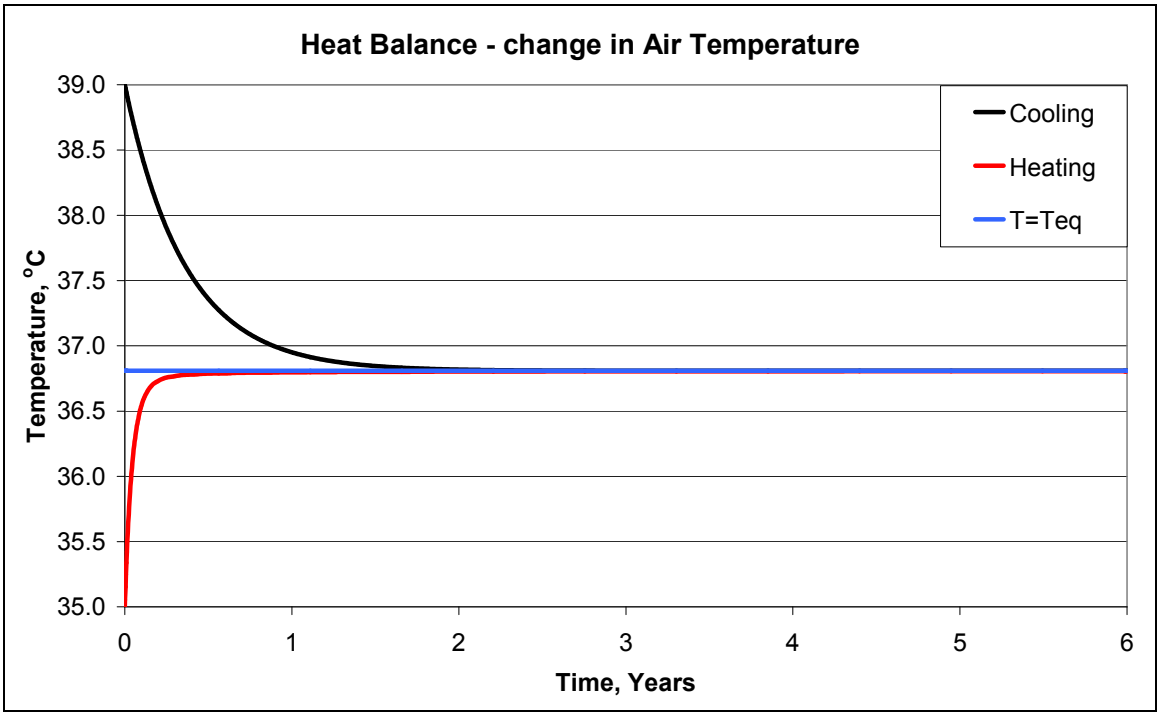

Figure 5.1.3. Model SST for input data with ambient air temperature that is higher than in the "base case" (see Table 5.1.1, run #2)

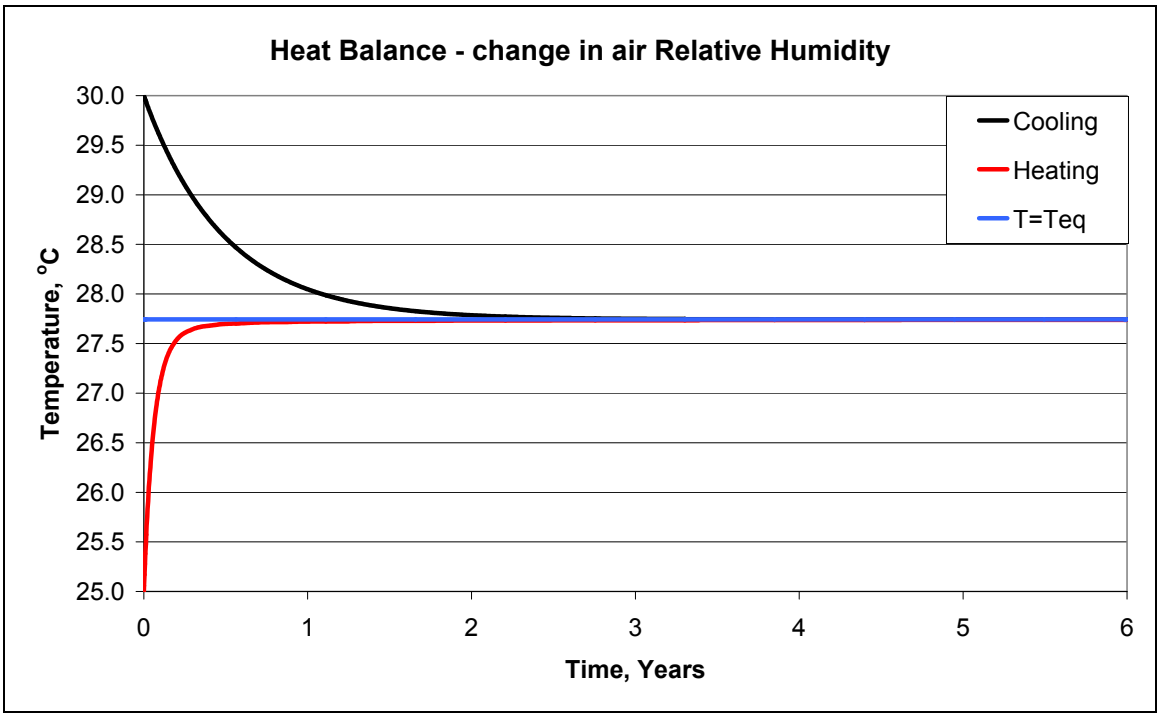

Figure 5.1.4. Model SST for input data with ambient air relative humidity that is lower than in the "base case" (see Table 5.1.1, run #3)

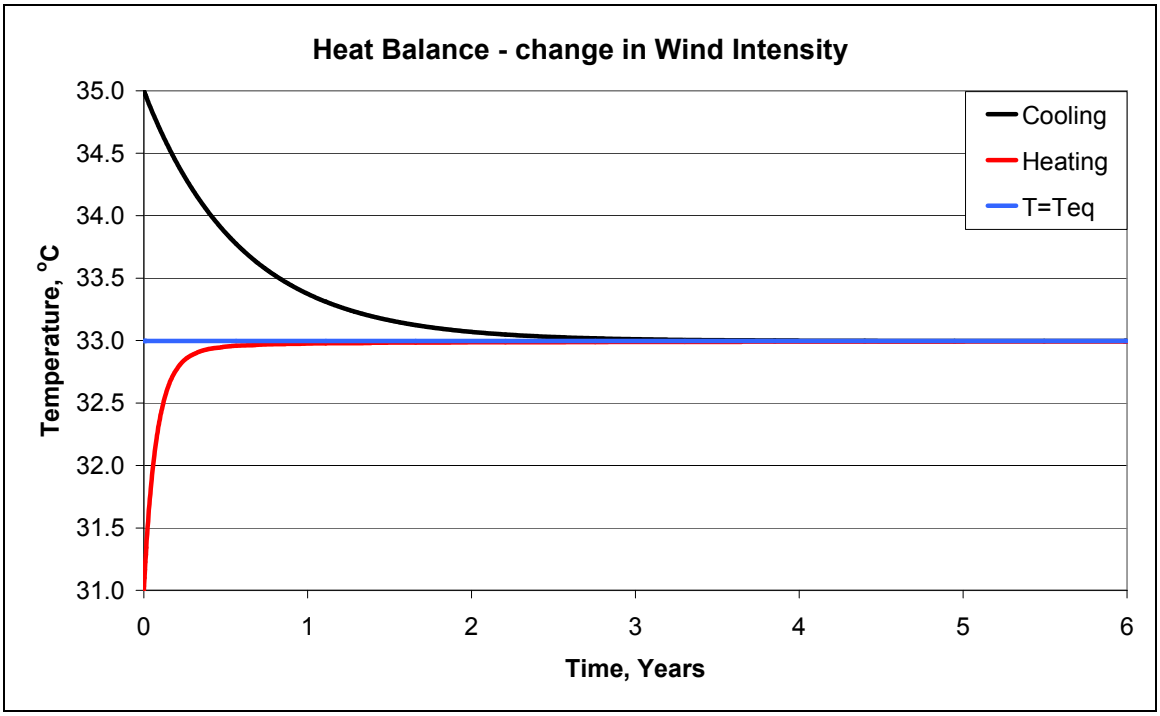

Figure 5.1.5. Model SST for input data with wind intensity that is lower than in the "base case" (see Table 5.1.1, run #4)

As expected, attainment of equilibrium when $T_i > T_{eq}$ takes longer than with $T_i < T_{eq}$. This is so because cooling involves the entire water column whereas during heating, thermal stratification develops and only the upper water column heats up. It should be noted that for each set of runs the final temperatures of heating and cooling are

slightly colder and hotter than T_{eq}, respectively. These reflect the asymptotic character of heating and cooling which still continue as the system approaches steady state. In all runs with $T_i=T_{eq,}$ the model maintained the equilibrium temperature for the duration of the run, i.e. for several years.

Even when the DS mass does not change, its level changes due to thermal expansion of the brine. Here we derive an analytical expression which enables to estimate this effect and compare it with numerical results. Following Eq. (4.0.1), and taking into account that $\Delta M_k = 0$ for all k, the water level change, Δz, due to temperature change is calculated by:

$$\Delta z = \sum_{k=1}^{KB} \Delta z_i^k \cdot \left(\frac{\rho_i^k}{\rho_f^k} - 1 \right), \qquad (5.1.1)$$

Where: $\Delta z^k{}_i$: initial thickness of the k-th cell,
KB: the number of cells,
ρ_i^k, ρ_f^k : initial and final densities of the k-th cell.

Denoting the overall depth of the Dead Sea as $H = \sum_{k=1}^{KB} \Delta z_i^k$ and taking into account that initially all cells have identical densities, $\rho_i^k \equiv \rho_i$, it follows that:

$$\Delta z = \rho_i \left(\sum_{k=1}^{KB} \frac{\Delta z_i^k}{\rho_f^k} \right) - H \qquad (5.1.2)$$

In the case of cooling, when the water column remains nearly homogeneous, the density can be treated as constant throughout the water column, $\rho_f^k \equiv \rho_f$, thus:

$$\Delta z = \frac{\rho_i}{\rho_f} \left(\sum_{k=1}^{KB} \Delta z_i^k \right) - H = H \left(\frac{\rho_i}{\rho_f} - 1 \right) \qquad (5.1.3)$$

Equation (5.1.3) implies that for the benchmarking of cooling, the water level drop can be estimated analytically from the initial conditions and meteorological parameters (i.e. T_{eq}) given that the Dead Sea mass and composition do not change. In contrast to cooling, surface heating results in stratification and therefore the level change cannot be calculated analytically. However, it is possible to estimate this level change by inserting the output of densities of the model into eq. (5.1.2), and compare it with the level change calculated by the model.

Tables 5.1.2 and 5.1.3 compare the numerical and analytically calculated temperatures, densities and water level change for runs of cooling and heating, respectively. These benchmark results, along with Figs. 5.1.1 to 5.1.5, clearly indicate that 1D-DS-POM runs properly and results in the expected (analytical) values. Thus, the heat module incorporated into the model works well and responds correctly to all input variables.

Table 5.1.2. Cooling results: T_i- initial temperature; ρ_i- the independently calculated initial brine density (using an Excel file checked against results provided by Prof. Kumgalz in private correspondence), ρ^*- initial density calculated by the model. T_{eq}- equilibrium temperature, T_f^*- average final temperature of the water column; ρ_f, ρ_f^*- independently calculated and model average final densities, respectively; Δz, Δz^*- analytically calculated – using eq. (5.1.3) – and model values of level change, respectively.

	Base Case	Short Wave Radiation (run #1)	Air Temperature (run #2)	Relative Humidity (run #3)	Wind Intensity (run #4)
T_i, ^oC	34.0	32.5	39.0	30.0	35.0
ρ_i, kg m^{-3}	1232.8363	1233.5722	1230.3477	1234.7776	1232.3419
ρ^*, kg m^{-3}	1232.8363	1233.5722	1230.3477	1234.7776	1232.3419
T_{eq}, ^oC	32.0721	30.3933	36.8083	27.7440	32.9965
T_f^*, ^oC	32.0723	30.3934	36.8085	27.7442	32.9967
ρ_f, kg m^{-3}	1233.7806	1234.5901	1231.4426	1235.8338	1233.3295
ρ_f^*, kg m^{-3}	1233.7806	1234.5900	1231.4425	1235.8337	1233.3294
Δz, m	-0.1607	-0.1732	-0.1867	-0.1795	-0.1682
Δz^*, m	-0.1607	-0.1731	-0.1867	-0.1795	-0.1682

Table 5.1.3. Heating results (See Table 5.1.2 for parameter descriptions). Δz – level change calculated from (5.1.2) based on model densities; Δz^* – level change calculated by the model, $<\Delta z^*>$ level change calculated analytically from (5.1.3) based on the average value of the final density.

	Base Case	Short Wave Radiation (run #1)	Air Temperature (run #2)	Relative Humidity (run #3)	Wind Intensity (run #4)
T_0, ^oC	30.0	28.5	35.0	25.0	31.0
ρ_0, kg m^{-3}	1234.7776	1235.4838	1230.3477	1234.7776	1232.3419
ρ^*, kg m^{-3}	1234.7776	1233.5722	1230.3477	1234.7776	1232.3419
T_{eq}, ^oC	32.0721	30.3933	36.8083	27.7440	32.9965
$<T_f^*>$, ^oC	30.4238	28.8730	35.3752	25.5460	31.4098
ρ_f, kg m^{-3}	1233.7806	1234.5901	1231.4426	1235.8338	1233.3295
$<\rho_f^*>$, kg m^{-3}	1234.5738	1235.3079	1232.1554	1236.8188	1234.1003
Δz, m	0.03469	0.02993	0.03181	0.04150	0.03387
Δz^*, m	0.03469	0.02993	0.03181	0.04150	0.03387
$<\Delta z^*>$, m	0.03467	0.02991	0.03180	0.04146	0.03385

5.2 Mass balance

The mass of the DS is influenced by the following processes: salt precipitation (SP), evaporation and inflows. The latter include fresh water (rain and flash floods, FWI), regular seawater (SWI), concentrated sea water (CSW) and end brines return (EB). In addition, the chemical industries pump brine from the lake (PMP). The proper incorporation of each of these processes in 1D-DS-POM was checked separately. While the processes influencing the different masses were found to be correctly implemented, the mass was not always fully conserved. Detailed analyses of run results indicate that these changes arise due to the numerical process of linear interpolation included in the remeshing procedure. Overall the change in mass due to remeshing is small to negligible (on the order of 10^{-3} % over a one year run; see Sections 4.1.1 and 5.3).

The following benchmarking was carried out assuming a constant area for the Dead Sea throughout the entire run. This allows comparing masses which are normalized to 1 m^2.

5.2.1 Salt Precipitation

Benchmarking of SP is based on the original C++ code by Krumgalz, which calculates the amount of precipitated salt. In Krumgalz's program, salt is precipitated from the oversaturated brine by an iterative process, which handles also high degrees of oversaturation. Salt precipitation is simulated there at small increments followed by renewed calculation of the degree of saturation. This continues until saturation is attained. In contrast, 1D-DS-POM "precipitates" salt in a single step (section 3.4). In order to verify that the numerical approach developed and incorporated in 1D-DS-POM runs properly, model results were compared to those calculated by Krumgalz's program.

A. Halite precipitation

The calculated weight of halite that precipitated from halite-oversaturated DS brine and the composition after attainment of saturation at 22°C were compared between runs with Krumgalz program and 1D-DS-POM code. The 1D-DS-POM run began with a homogeneous water column which was set to a temperature of 23.01 °C, for which the initial composition is slightly undersaturated with respect to halite. By switching off the SW radiation, the water column was allowed to slowly cool down, attain saturation and precipitate halite. As outlined in section 5.1, cooling of the water column under these conditions ensures that it remains homogeneous. In this run, no water inflow, pumping or evaporation were allowed. The parameters of the heat balance were constant with time: Q_{SW} = 0 Wm^{-2}, T_a = 20°C, RH = 66%, WI = 5.35 ms^{-1} (WF = 8.9).

Table 5.2.1 presents the brine composition, in molalities, before and after salt precipitation, along with the corresponding halite saturation degrees calculated by the two codes. The results presented for 1D-DS-POM are those for the water column at the time it has cooled down to 22°C. Also included is the weight of halite that was "precipitated" by the codes to attain saturation. As presented in the Table, Krumgalz program completed halite precipitation when the brine attained saturation degree of 0.99992. Thus, in order to allow comparison between model output and Krumgalz

code, the threshold degree of saturation in 1D-DS-POM was reduced to Ω^0_{sat} =0.99992, with the excess over saturation, ε, set to 10^{-6} (see Section. 3.4).

Another way of verifying the correctness of the calculation of halite precipitation is through mass balances. 1D-DS-POM tracks the mass of each of the dissolved ions in solution as well as the total weight of salt that precipitated from the brine. Thus, it is possible to compare the initial and final masses of dissolved sodium (Na) and chloride (Cl) and compare it with the mass of halite that was precipitated by the model. Such comparison is of course valid only if no additional processes, such as inflow, pumping or end brine discharge, are involved. In the present benchmarking run, these were excluded. Comparison between initial and final masses of Na and Cl in the brine indicates that 31.209 and 48.128 Kg of Na and Cl, respectively, have been removed from the brine. Added together, these masses are equivalent to the calculated mass of halite that was precipitated by 1D-DS-POM. Finally, the Na/Cl mass ratio of the "missing" Na and Cl is 0.6485, which is the ratio in halite, further indicating that the program correctly removes halite from the brine. Thus, we conclude that the model "precipitates" halite correctly to attain saturation, and correctly records the weight of halite it precipitated. The composition of the brine at the end of this process is consistent with the amount of halite that was precipitated.

Table 5.2.1. Brine composition, in molalities, before and after halite precipitation, along with the corresponding saturation degrees and densities calculated by the two codes.

	Initial conditions	Krumgalz (C++) code output	1D-DS-POM output
Na	1.7606	1.7534	1.7534
K	0.2239	0.2239	0.2239
Ca	0.5007	0.5007	0.5007
Mg	2.1327	2.1327	2.1327
Cl	7.1663	7.1591	7.1591
Br	0.07675	0.07675	0.07675
HCO_3	0.00501	0.00501	0.00501
SO_4	0.002727	0.002727	0.002727
ρ_i (T=23.01 ^oC)	1237.9057	N/A	N/A
ρ_f (T=22.00 ^oC)	N/A	1238.1267	1238.1267
Ω_{halite} (22°C)	1.006897	0.99992	0.99992
Ω_{gypsum} (22°C)	0.995602	0.993349	0.993383
Precipitated halite (Kg)	N/A	79.338*	79.337
level change due to ion removal (m)	N/A	0.10147**	0.10149

*In Krumgalz's C++ code the output for the amount of halite precipitation is provided in units of mole/Kg H_2O (0.007216). This value was translated to the weight of halite that precipitates from a water column with 1 m^2 area by multiplying it by the mass of H_2O in the column and the molecular weight of halite.
** Calculated analytically.

Salt precipitation affects water level in two opposite ways: 1) level rises due to the halite that accumulates on the seafloor; 2) level drops due to decrease in the mass of brine following the removal of the dissolved ions (the lowered mass is translated to a smaller brine volume). It should be noted that the decrease in the density of the brine due to salt precipitation is translated to some level rise (see Eq. 4.0.1). However, this factor impacts much less on the water level than the impact of decreased brine mass. The processes which affect water level were checked by separately following their corresponding impact on water level change:

- level rise due to salt accumulation, Δz^{+}, can be evaluated by:

  $\Delta z^{+} = M_{salt}/\rho_{salt}$

  where M_{salt} is the calculated mass that precipitated from the water column (Kg m^{-2}) and ρ_{salt} is the density of halite. Given halite density of 2170 Kg/m^3, the 79.337 Kg m^{-2} of halite that precipitated correspond to 0.0366 m level rise. This value is identical to the level rise calculated by the model.

- The level change due to the removal of dissolved ions from the brine is calculated following Eq. (4.0.1). Since both the initial and final densities of the brine are known, the expected level change can be calculated analytically (see impact of cooling in the heat balance benchmarking). The initial and final densities were determined using the Excel file using the initial and final compositions and temperatures (see Table 5.2.1). The analytically calculated level change, Δz, was found to be Δz=-0.10147 m, very similar to the model output of Δz=-0.10149 m. Thus halite precipitation works as expected.

B. Gypsum precipitation

Benchmarking for gypsum precipitation was carried out similarly to that of halite. To ensure that gypsum precipitation will start before that of halite, the molal concentrations of Na and Cl in the composition of the Dead Sea were decreased by $0.1m$. The threshold saturation value for gypsum precipitation was set as $\Omega^{0}_{sat} = 1$. The excess over saturation, ε, was set at 10^{-4}. C++ calculations were carried out at 20°C. The results are summarized in Table 5.2.2.

The model was modified exactly as in the benchmarking for halite precipitation. For the given composition, gypsum precipitation starts at 20.819°C. Accordingly, the initial temperature of the water column in 1D-DS-POM was set to 20.82°C. The model reaches the prescribed temperature of 20°C in about 80 days. The amount of precipitated gypsum is 2.19079 Kg, in satisfactory agreement with Krumgalz's model.

The change in DS level due to gypsum precipitation was checked similarly to that following halite precipitation. Analytical and model values of level rise were found to be identical. The values for level fall due to ion removal are nearly identical (Table 5.2.2).

The masses of Ca, SO_4 and H_2O which have been removed from the brine by the end of the run are 0.509994, 1.22228 and 0.458467 Kg, respectively. Summed together their mass is 2.19074 Kg of gypsum which is $1.26\cdot10^{-3}$ Kg (1.26 g) short of the calculated weight of precipitated gypsum. The mole ratio of these components is 1:1:2, in agreement with the stoichiometric composition of gypsum ($CaSO_4\cdot2H_2O$).

To conclude, the thermodynamic calculations for gypsum precipitation have been satisfactorily incorporated into 1D-DS-POM.

Table 5.2.2. Brine composition, in molalities, before and after gypsum precipitation, along with the corresponding saturation degrees calculated by the two codes.

	Initial conditions	C++ code output	1D-DS-POM output
Na	1.660635	1.660639	1.660639
K	0.223871	0.223872	0.223872
Ca	0.500745	0.500679	0.500679
Mg	2.132695	2.132700	2.132700
Cl	7.066274	7.066291	7.066291
Br	0.076754	0.076754	0.076754
HCO_3	0.005009	0.005009	0.005009
SO_4	0.002727	0.002660	0.002659
ρ_i (T=20.82 ^oC)	1236.1546	N/A	N/A
ρ_f (T=20.00 ^oC)	N/A	1236.4537	1236.4538
Ω_{halite} (20°C)	0.92570	0.925687	0.925692
Ω_{gypsum} (20°C)	1.02557	1.00007	1.000000003
Precipitated gypsum (Kg)	N/A	2.192*	2.191
level change due to ion removal (m)	N/A	0.05258**	0.05259

*calculated from 6.7479E-5 moles gypsum/1Kg H_2O (see Table 5.2.1).
** Calculated analytically

5.2.2 Evaporation

Evaporation, which is part of the heat flux calculations, impacts on several additional processes in the code, including sea level change and water mass balance. The correct incorporation of these into the code is evaluated as follows:

1) Given the bulk energy that goes into evaporation, and knowing the latent heat, it is possible to analytically determine the weight of water that evaporates. This value can be compared to model results.
2) The weight of the evaporated water is compared to two related values: the decrease in the mass of H_2O in the Dead Sea and the overall decrease in the Dead Sea mass.
3) Evaporation should not change the dissolved masses of ions in the brine. Thus, their masses at the onset and end of model runs can be compared.
4) Given the weight of evaporated water, it is possible to analytically calculate the new molalities of all constituents and compare them to model results.
5) Given the new molalities and hence density of the brine, and taking into account that evaporation leaves the column homogeneous, the level change can be calculated analytically (using Eq. 4.0.1). This value can be compared to model results.

In order to carry out the above benchmarking, the model was modified as follows:

a) A constant meteorology input data was provided along with SST = T_{eq} (Table 5.1.1 first row).

b) No inflows or pumping were allowed.

c) A constant water activity (see Table 5.1.1, first row) was assumed (which otherwise changes due to increasing temperature and salinity of the brine). This ensures a constant rate of evaporation in spite of changing water activity.

d) Salt precipitation was disabled.

e) No penetrative radiation was allowed i.e. the short wave radiation was fully absorbed in the upper cell.

f) As was mentioned earlier, water level drop or rise do not change the surface area of the DS.

As expected, under the above model modifications, SST remained unchanged for the duration of model run (10 years).

Since all meteorological parameters as well as water activity (the only variable that depends on the parameters of the brine) are maintained constant, the heat of evaporation, EH (which is a function of water activity, wind function and saturated water vapor pressure at the temperatures of sea surface and ambient air, see Eq. 2.1.2), is also constant.

The evaporative heat for the given meteorological parameters is EH= 83.625 Wm^{-2}. Given the Dead Sea latent heat of evaporation of LH=2,489,480 J/Kg (Steinhorn, 1981), the rate of evaporation is $3.359 \cdot 10^{-5}$ Kg m^{-2} sec^{-1}. The weights of evaporated water over the 10 years period calculated analytically and modeled by 1D-DS-POM were identical and found to be 10,593 Kg. The decrease in the H_2O mass as well as the decrease in the overall Dead Sea mass were identical to the weight of the evaporated water (to within ($3 \cdot 10^{-4}$ %, the difference probably arising from numerical noise). Thus, the mass balance for evaporation is correctly incorporated in the code.

Evaporation also impacts on the molal concentration of the chemical constituents and the density of the brine. Results of the 10 year model run are nearly identical to the analytically determined values, the difference not exceeding 0.004%. Exceptions to this are the two constituents with the lowest concentrations (HCO_3 and SO_4), for which the difference does not exceed 0.01%. The difference in the analytical and model densities is $2 \cdot 10^{-5}$%. Finally, following Eq. (4.0.1), the level drop during the 10 years runs should be 10.474 m. Model result differs from this value by only $3 \cdot 10^{-4}$ m, (i.e. difference of about 0.003%).

To conclude, the benchmarking of evaporation indicates that it is incorporated correctly into 1D-DS-POM.

5.2.3 Inflows

Five inflow sources are considered: 1) Fresh water (FW), 2) Seawater (SW), 3) reject brine from desalinization (RB) 4) End brine discharge from the chemical industries (EB) and 5) pumping of DS brines by the chemical industries. The latter can be considered as a negative inflow, which is treated in the model similarly to all other inflows.

The inflow volumes for each of the sources are provided in units of m^3/sec on a monthly basis accompanied by a characteristic temperature. This allows varying the flow rates every month. In order to avoid step-like changes in inflow volume and temperature, the program calculates the input volume and temperature for each time step by interpolation. The two end points for the interpolation are the inflow volumes in the last and first 10 days of the two adjacent months, respectively. Exceptions to this are the beginning of January of the first year and the end of December of the last year of the run, when no interpolation is done and the inflow is taken to be that of the corresponding input inflow.

In the benchmarking of inflows, no heat exchange and thus evaporation was allowed and the temperatures of the inflows were set to that of the given DS temperature (20°C). Benchmarking for inflows were carried out separately for each of the five sources. In each run, only a single inflow source was provided and all others sources were switched off. At the end of the runs the following were checked:

Is the volume of inflow given in the input file translated correctly by the code?

Is inflow volume translated correctly to inflow mass (the inflow density is known since its temperature is known) and treated correctly by the code?

Does sea level rise in accord with the inflow volume and density?

Is the increase in the masses of the water and chemical components in the lake equal to the masses introduced to the lake by the inflow?

Is the increase in the total mass of the DS identical to the total mass of the inflow?

All inflows were introduced at the same rate, which varied each month, thereby allowing also checking the interpolation between adjacent months and between consecutive years. Runs were carried out for 10 years. Table 5.2.3 presents these monthly rates (given in m^3/s), which cumulatively are equivalent to annual inflow rate of about 763 MCM.

Table 5.2.3. Monthly inflow rates in m^3/s used in the benchmarking of inflows.

Month	Jan	Feb	Mar	Apr	May	Jun	Jul	Aug	Sep	Oct	Nov	Dec
Inflow	10	20	20	30	30	30	40	30	20	10	20	30

Volume of Inflow

The inflow volume provided as input was compared to the calculated model cumulative inflow volume over all time steps, i.e.:

$$V_{total} = \sum_{time} V_{time}$$

The model calculated correctly this volume over a single year and in 10 year runs for all sources of inflows.

Mass of Inflows

Given the inflow masses and their densities (as determined from their temperatures and chemical compositions), it is possible to calculate the masses added to the lake via the inflow. This inflow mass is followed independently in the code and was found to fully comply, in all runs, with the analytically determined inflow mass. The densities at the inflow temperature of 20°C are: ρ_{FW} = 998.20 Kg m^{-3}; ρ_{SW} = 1031.5 Kg m^{-3}; ρ_{RB} = 1062.6 Kg m^{-3}; ρ_{EB} = 1329.3 Kg m^{-3}.

Change in water level due to pumping and inflow

All inflows involve change in the density of the Dead Sea brine. Thus, the change in the water level due to the inflows cannot be determined analytically and therefore must be estimated. Such estimation is based on the density profiles obtained from the benchmarking runs. This profile is translated to an averaged density, $\overline{\rho}$, for the entire water column:

$$\overline{\rho} \equiv \frac{1}{KB}\sum_{k=1}^{KB}\rho^k ,$$

where KB is the number of cells and ρ^k is the density of the cell number *k*.

The change in the Dead Sea due to inflow is estimated using the following equation:

$$\Delta z = H_{fin} - H_{ini} = \frac{M_{fin}}{\overline{\rho}_{fin}} - \frac{M_{ini}}{\overline{\rho}_{ini}} = \frac{\Delta M}{\overline{\rho}_{fin}} + H_{ini}\left(\frac{\overline{\rho}_{ini}}{\overline{\rho}_{fin}} - 1\right), \quad (5.2.1)$$

Where: H_{ini} and H_{fin} are the initial and final normalized Dead Sea depths and $\overline{\rho}_{ini}$, $\overline{\rho}_{fin}$ are the initial and final average density of the brine, respectively.

Unlike the inflows, the water level change due to pumping can be determined analytically because this process involves no change in the density of the brine. Thus, water level change is calculated directly from the volume and the density of the brine being pumped from the lake.

Table 5.2.4 compares the model and the estimated level changes for each inflow.

Mass added to the Dead Sea

The mass of inflow, calculated correctly by the model, should also be reflected in the change in the mass of the Dead Sea. The latter can be calculated from the volume and density of the individual cells:

$$M_{DS} = \sum_{cell} V_{cell}\rho_{cell}$$

The mass added to the Dead Sea via inflow during the run is thus determined by comparing the initial and final masses of the DS:

$$\Delta M_{DS} = M_{DS-final} - M_{DS-initial}$$

Table 5.2.4 includes a comparison between the analytically calculated and model output of the masses added to the Dead Sea during the runs. The small (<0.01%)

deviation from the analytically calculated change in mass is attributed to remeshing which is known to be non-mass conserving (section 4.1.1).

The minute difference in the analytically calculated or estimated values vs. the output from the 10 year model runs suggest that the inflows (and pumping), including mass and density changes and impact on water level are incorporated correctly into 1D-DS-POM.

Table 5.2.4. Comparison between analytically calculated (A) and model results (M) of the impact of different types of inflows. The run conditions over the 10 year period are outlined in the text. Variables compared include: level change (LC), mass of 1 m^2 of the Dead Sea (M_{DS}), total mass of water in the DS brine (H_2O), total weight of dissolved ions (Σ Ions) and the individual ions. Also included are the absolute (Δ) and the relative (in parenthesis) differences between each two calculations.

		FW Inflows	SW Inflows	RB	EB	Pumping
LC, m	A	11.497	11.546	11.581	11.617	11.647
	M	11.494	11.542	11.577	11.618	11.647
	Δ, m (%)	$3\cdot10^{-3}$ (0.03)	$4\cdot10^{-3}$ (0.03)	$4\cdot10^{-3}$ (0.03)	$2\cdot10^{-4}$ (<0.01)	0
M_{DS} Kg m^{-2}	A	$2.7186\cdot10^5$	$2.7225\cdot10^5$	$2.7261\cdot10^5$	$2.7571\cdot10^5$	$2.4580\cdot10^5$
	M	$2.7185\cdot10^5$	$2.7224\cdot10^5$	$2.7260\cdot10^5$	$2.7571\cdot10^5$	$2.4580\cdot10^5$
	Δ, Kg (%)	4.1 (<0.01)	5 (<0.01)	4.8 (<0.01)	-0.3 (<0.01)	0
H_2O; Kg m^{-2}	A	$1.9994\cdot10^5$	$1.9980\cdot10^5$	$1.9964\cdot10^5$	$1.9837\cdot10^5$	$1.7787\cdot10^5$
	M	$1.9994\cdot10^5$	$1.9980\cdot10^5$	$1.9964\cdot10^5$	$1.9836\cdot10^5$	$1.7787\cdot10^5$
	Δ, Kg (%)	-4.6 (<0.01)	-4.8 (<0.01)	-3.6 (<0.01)	-0.2 (<0.01)	0
Σ Ions Kg m^{-2}	A	$7.1917\cdot10^5$	$7.2449\cdot10^5$	$7.2966\cdot10^5$	$7.7347\cdot10^5$	$6.7929\cdot10^5$
	M	$7.1909\cdot10^5$	$7.2440\cdot10^5$	$7.2957\cdot10^5$	$7.7347\cdot10^5$	$6.7929\cdot10^5$
	Δ, Kg (%)	8.8 (0.01)	8.7 (0.01)	8.4 (0.01)	0.09 (<0.01)	0
Na, Kg m^{-2}	A	$7.6223\cdot10^3$	$7.7846\cdot10^3$	$7.9425\cdot10^3$	$7.6625\cdot10^3$	$7.1996\cdot10^3$
	M	$7.6214\cdot10^3$	$7.7839\cdot10^3$	$7.9422\cdot10^3$	$7.6625\cdot10^3$	$7.1996\cdot10^3$
	Δ, Kg (%)	0.9 (0.01)	0.6 (<0.01)	0.3 (<0.01)	0.006 (<0.01)	0
K, Kg m^{-2}	A	$1.6483\cdot10^3$	$1.6540\cdot10^3$	$1.6596\cdot10^3$	$1.6890\cdot10^3$	$1.5569\cdot10^3$
	M	$1.6481\cdot10^3$	$1,6538\cdot10^3$	$1.6594\cdot10^3$	$1.6890\cdot10^3$	$1.5569\cdot10^3$
	Δ, Kg (%)	0.2 (0.01)	0.2 (0.01)	0.2 (0.01)	0.002 (<0.01)	0
Ca, Kg m^{-2}	A	$3.7794\cdot10^3$	$3.7856\cdot10^3$	$3.7916\cdot10^3$	$4.2030\cdot10^3$	$3.5699\cdot10^3$
	M	$3.7790\cdot10^3$	$3,7850\cdot10^3$	$3.7910\cdot10^3$	$4.2030\cdot10^3$	$3.5699\cdot10^3$
	Δ, Kg (%)	0.5 (0.01)	0.5 (0.01)	0.6 (0.02)	0.01 (<0.01)	0
Mg, Kg m^{-2}	A	$9.7613\cdot10^3$	$9.7807\cdot10^3$	$9.7996\cdot10^3$	$1.0771\cdot10^4$	$9.2200\cdot10^3$
	M	$9.7601\cdot10^3$	$9.7794\cdot10^3$	$9.7982\cdot10^3$	$1.0771\cdot10^4$	$9.2200\cdot10^3$
	Δ, Kg (%)	1.2 (0.01)	1.3 (0.01)	1.4 (0.01)	0.02 (<0.01)	0

Cl, Kg m^{-2}	A	$4.7844 \cdot 10^4$	$4.8142 \cdot 10^4$	$4.8431 \cdot 10^4$	$5.1631 \cdot 10^4$	$4.5191 \cdot 10^4$
	M	$4.7838 \cdot 10^4$	$4.8136 \cdot 10^4$	$4.8425 \cdot 10^4$	$5.1631 \cdot 10^4$	$4.5191 \cdot 10^4$
	Δ, Kg (%)	5.8 (0.01)	5.9 (0.01)	5.9 (0.01)	0.06 (<0.01)	0
Br, Kg m^{-2}	A	$1.1549 \cdot 10^3$	$1.1558 \cdot 10^3$	$1.1566 \cdot 10^3$	$1.2755 \cdot 10^3$	$1.0909 \cdot 10^3$
	M	$1.1548 \cdot 10^3$	$1.1556 \cdot 10^3$	$1.1564 \cdot 10^3$	$1.2755 \cdot 10^3$	$1.0909 \cdot 10^3$
	Δ, Kg (%)	0.1 (0.01)	0.2 (0.01)	0.2 (0.02)	0.002 (<0.01)	0
HCO_3, Kg m^{-2}	A	57.555	59.709	61.805	63.115	54.364
	M	57.548	59.706	61.807	63.115	54.364
	Δ, Kg (%)	0.007 (0.01)	0.002 (<0.01)	0.003 (<0.01)	$1 \cdot 10^{-4}$ (<0.01)	0
SO_4, Kg m^{-2}	A	49.329	86.434	122.54	50.024	46.593
	M	49.323	86.513	122.72	50.024	46.593
	Δ, Kg (%)	0.006 (0.01)	-0.09 (0.09)	-0.2 (0.2)	$4 \cdot 10^{-5}$ (<0.01)	0

5.3 Compressible vs. Incompressible Models

To examine the importance of the compressibility in modeling of the Dead Sea and the RSDSC, 1D-DS-POM was degenerated so as to obtain an incompressible version (ignoring the second term in Eq. 2.3.2). One-year runs with identical initial and meteorological conditions were carried out with 1D-DS-POM and the degraded version. Runs included the present day 350 MCM/yr freshwater inflow and runs with additional freshwater inflow volume of 1000 MCM/yr (total of 1350 MCM/yr). Table 5.3.1 presents the results of the models comparison. The first three rows present the differences in model output for level change (Δz), temperature change (ΔT) and salinity change (ΔS) for the two inflow volumes. The last row, ΔM, presents the mass deficit relative to the analytically calculated mass of the DS at the end of the runs. This difference between 1D-DS-POM result and the analytical result is due to the non-mass conservative nature of grid remeshing. Figure 5.3.1 presents the level changes for the compressible and incompressible codes for the case of 1,350 MCM/yr fresh water inflows.

Table 5.3.1. Comparison of results from 1D-DS-POM (compressible- C) and the degenerated code (incompressible - IC) of the upper cell values and the overall mass deficit in runs with different volumes of freshwater inflows (FWI). ΔFin: difference at the end of the runs; ΔMax – the maximal difference during the year.

Inflows, MCM/yr	350				1350			
	C	IC	ΔFin	ΔMax	C	IC	ΔFin	ΔMax
level change, m	-1.106	-1.053	-0.053	-0.053	0.287	0.176	0.111	0.199
temperature change, ^{o}C	0.236	0.238	-0.017	0.037	0.660	0.657	0.003	0.016
salinity change, g/Kg	0.300	0.301	$-6\cdot10^{-4}$	0.015	-5.517	-5.521	0.004	0.008
Mass deficit, 10^{9}Kg	-3.5	39.8	-43.4	-43.4	-1.1	-91.3	-90.3	160.9

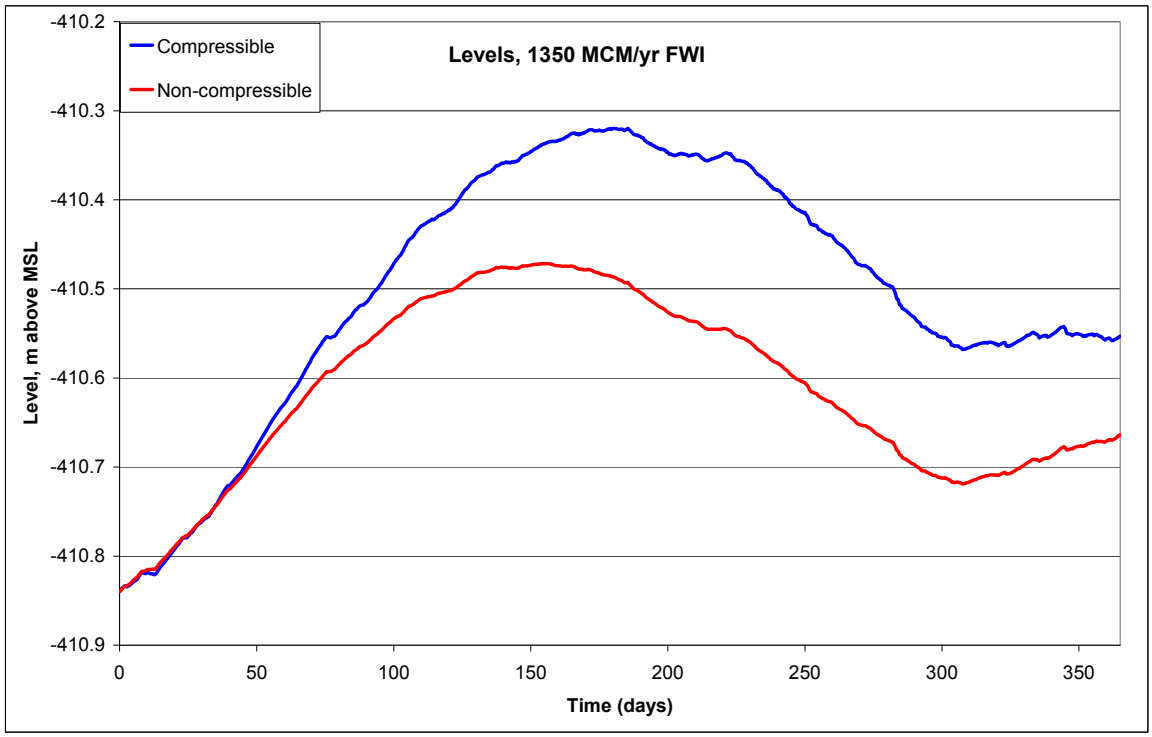

Figure 5.3.1 Level changes for 1,350 MCM/yr fresh water inflows.

As is readily seen from Table 5.3.1, salinity and temperature values calculated by the compressible (1D-DS-POM) and the incompressible codes are nearly identical. The difference in the mass deficit between the codes is relatively larger. Nevertheless, these deficits are a small fraction (no greater than 0.1%) of the overall DS mass ($1.7\cdot10^{14}$ Kg) and therefore may suggest that compressibility is not an important factor to be considered in future Dead Sea modeling. However, when considering level change, the compressibility effect is more important and accounts for 5% of the actual level change when freshwater inflows reach 1350 MCM/yr.

To conclude, the incompressible code works satisfactorily when dealing with relatively small water inflow, which has little effect on the density of the water column. However, when inflow volumes are increased, and the density of the water column changes significantly, the compressibility effects become important. Thus, at this stage 1D-DS-POM runs as a fully compressible code.

6 Summary

The unique chemical and physical properties of the DS impose a challenge in modeling its dynamics. Here we presented the structure and benchmarking results of 1D-DS-POM code, which is one dimensional limnological, compressible, multi-component, chemistry-based model for the DS.

The model tracks the concentrations, both in molalities [moles /(Kg H_2O)] and in weight units (g/Kg), of the major eight constituents of the Dead Sea (Na, K, Ca, Mg, Cl, Br, HCO_3, SO_4). The molality concentrations are used in the thermodynamics calculations that adopt the Pitzer thermodynamic approach. These calculations provide a) the density of the solution for a wide range of densities, from freshwater (1,000 Kg m^{-3}), to the end brines of the chemical industries (1,340 Kg m^{-3}); b) the brine's degree of saturation for three different salts (halite, NaCl; gypsum, $CaSO_4 \cdot 2H_2O$ and carnallite, $KMgCl_3 \cdot 6H_2O$) with subsequent salt precipitation in the case of oversaturation so that the saturation is regained, and c) the activity of H_2O in the brine, which is required for evaporative heat flux calculations. The concentrations in weight units are used to solve for the vertical turbulent mass transport using the Mellor-Yamada closure (1D-POM). The heat transport is calculated using the same approach with a boundary condition based on surface heat exchange.

Input to 1D-DS-POM includes measured meteorological data (air temperature, humidity, wind intensity and incoming short wave radiation), pumping volumes from the Dead Sea and inflows. The latter is composed of four different sources: freshwater, seawater, concentrated seawater (after desalination) and the industrial end brines. The presented benchmarking runs, which are mostly compared to analytical solutions or independent external models, demonstrates the ability of 1D-DS-POM to correctly reproduce the dynamics of the Dead Sea with different volumes and kinds of inflows and pumping.

Future runs will examine the sensitivity of the model results to various parameters controlling the physical processes that are modeled and the model will be calibrated against available limnological data for the past years. Once calibrated, long term runs (i.e. 50 years) will be carried out to model the future evolution of the Dead Sea under different scenarios, including massive inflow of seawater.

Acknowledgement

We wish to thank Scott Wells for his detailed review and suggestions which greatly improved the report. The development of the code and the presented study was partly funded by the U.S. Agency for International development, the Middle East Regional Cooperation program (MERC project TAMOU-03-M23-024), and by a grant of the Israel Science Foundation (grant 902/05 to IG).

7 References

Anati, D.A., (1997): The hydrography of a hypersaline lake. In: The Dead Sea: The Lake and Its Settings, T. Niemi, Z. Ben-Avraham, and J.R. Gat, eds. *Oxford Univ. Press, New York,* pp. 89-103.

Cole, T.M. and S. Wells, (2006): CE-QUAL-W2: A Two-Dimensional, Laterally Averaged, Hydrodynamic and Water Quality Model, Version 3.5

Ganor, J., I. Gavrieli and I. Reznik, (2006): The kinetics of gypsum precipitation due to seawater – Dead Sea mixing and the possibility of "whitening" of the surface water (in Hebrew). *Isr. Geol. Surv., Rep*. GSI/32/06 & *Minist. Nation. Infrastructures Rep*., ES-28-2006.

Gavrieli, I., A. Bein and A. Oren, (2005): The deteriorating Dead Sea basin: limnological and environmental changes and the expected impact of the "Peace Conduit". *Mitigation and Adaptation Strategies for Global Change,* 10(1), 3-22. Erratum: p. 739 and pp. 759-777

Gavrieli I., N. Lensky, N. Gazit-Yaari and A. Oren, (2002): The impact of the proposed "Peace Conduit" on the Dead Sea- Evaluation of current knowledge on Dead Sea – seawater mixing. *Isr. Geol. Surv., Rep.* GSI/23/02

Gavrieli I., N. Lensky, Y. Dvorkin, V. Lyakhovsky and I. Gertman, (2006): A multi-component chemistry-based model for the Dead Sea. Modification to the 1D Princeton Oceanographic Model. *Isr. Geol. Surv., Rep.* GSI/24/06.

Krumgalz, B.S., (2001): Application of the Pitzer ion interaction model to natural hypersaline brines. *Journal of Molecular Liquids*, 91, pp. 3-19

Krumgalz, B.S. and F.J. Millero, (1982): Physico-chemical study of the Dead Sea waters. *Marine Chemistry***,** 11, pp. 209-222.

Krumgalz, B.S., R. Pogorelsky, A. Sokolov and K.S. Pitzer, (2000): Volumetric ion interaction parameters for single-solute aqueous electrolyte solutions at various temperatures. *J. Phys. Chem. Ref. Data,* **29**(5), pp 1123-40.

Krumgalz, B.S., R. Pogorelsky, and K.S. Pitzer, (1995): Ion interaction approach to calculations of volumetric properties of aqueous multiple-solute electrolyte solutions. *J. Solut. Chem.,* 24, pp 1025-38.

Lensky, N.G., Y. Dvorkin, V. Lyakhovsky, I. Gertman, and I. Gavrieli, (2005): Water, salt, and energy balances of the Dead Sea, *Water Resources. Research.,* 41, W12418, doi:10.1029/2005WR004084

Mellor, G.L., (2004): Users Guide for a Three-Dimensional, Primitive Equation, Numerical Ocean Model, (http://www.aos.princeton.edu/WWWPUBLIC/htdocs.pom/FTPbackup/usersguide0604.pdf)

Oren A., Gavrieli I., Gavrieli J., Kohen M., Lati J. and Aharoni M. (2004): Biological effects of dilution of Dead Sea brine with seawater: implications for the planning of the Red Sea – Dead Sea "Peace Conduit". *J. Marine Systems,* 46, 121-131. doi:10.1016/j.jmarsys.2003.11.017

Oren A., Gavrieli I., Gavrieli J., Kohen M., Lati J. and Aharoni M. (2005): Long term biological simulation experiments of mixing Red Sea waters with Dead Sea brines, and the effect of antiscalants on the biology of the Dead Sea. *Isr. Geol. Surv., Rep.* GSI/28/05.

Pitzer, K.S., (1991): Ion interaction approach: theory and data correlation. In: Activity Coefficients in Electrolyte Solutions. 2nd ed. K.S Pitzer (ed.) *CRC Press,* pp 75-153.

Steinhorn, I. (1981): A hydrographical and physical study of the Dead Sea during destruction of its long-term meromictic stratification, *Ph.D. thesis, Weizmann* Inst. of Sci., Rehovot, Isr.